Biochimica et Biophysica Acta 1823 (2012) 1877–1893

Contents lists available at SciVerse ScienceDirect

Biochimica et Biophysica Acta

journal homepage: www.elsevier.com/locate/bbamcr

The major isoforms of Bim contribute to distinct biological activities that govern the processes of autophagy and apoptosis in interleukin-7 dependent lymphocytes

Shannon M. Ruppert [a], Wenqing Li [b], Ge Zhang [a], Adina L. Carlson [a], Arati Limaye [a], Scott K. Durum [b], Annette R. Khaled [a,*]

[a] Burnett School of Biomedical Sciences, College of Medicine, University of Central Florida, Orlando, FL 32827, USA
[b] National Cancer Institute at Frederick, Frederick, MD 21702, USA

ARTICLE INFO

Article history:
Received 30 December 2011
Received in revised form 1 June 2012
Accepted 14 June 2012
Available online 21 June 2012

Keywords:
Bcl-2
Cytokine
Lysosome
Fluorescence
Acidification
Dynein

ABSTRACT

Bim is a BH3-only member of the Bcl-2 family that enables the death of T-cells. Partial rescue of cytokine-deprived T-cells occurs when Bim and the receptor for the T-cell growth factor, interleukin-7, are deleted, implicating Bim as a possible target of interleukin-7-mediated signaling. Alternative splicing yields three major isoforms: BimEL, BimL and BimS. To study the effect of Bim deficiency and define the function of the major isoforms, Bim-containing and Bim-deficient T-cells, dependent on interleukin-7 for growth, were used. Loss of total Bim in interleukin-7-deprived T-cells resulted in delayed apoptosis. However, loss of Bim also impeded the later degradative phase of autophagy. p62, an autophagy-adaptor protein which is normally degraded, accumulated in Bim deficient cells. To explain this, BimL was found to support acidification of lysosomes that later may associate with autophagic vesicles. Key findings showed that inhibition of lysosomal acidification accelerated death upon interleukin-7 withdrawal only in Bim-containing T-cells. intereukin-7 dependent T-cells lacking Bim were less sensitive to inhibition of lysosomal acidification. BimL co-immunoprecipitated with dynein and Lamp1-containing vesicles, indicating BimL could be an adaptor for dynein to facilitate loading of lysosomes. In Bim deficient T-cells, lysosome-tracking probes revealed vesicles of less acidic pH. Over-expression of BimL restored acidic vesicles in Bim deficient T-cells, while other isoforms, BimEL and BimS, promoted intrinsic cell death. These results reveal a novel role for BimL in lysosomal positioning that may be required for the formation of degradative autolysosomes.

1. Introduction

Cell death is an essential process needed for tissue homeostasis. Central to the modulation of apoptotic death are members of the B-cell lymphoma-2 (Bcl-2) family, which includes pro-survival proteins, such as Bcl-2 and Bcl-xL, pro-apoptotic members, like the multi-domain proteins, Bax and Bak, and a number of BH3-only proteins, such as Bad, Bid, Bim or Bmf [1]. Of the BH3-only proteins, Bim emerges as an important regulator of T-lymphocyte (T-cell) apoptosis. Bim is necessary for the death of autoreactive T-cells and is upregulated in T-cells upon death induced by T-cell receptor re-stimulation or growth factor withdrawal [2,3]. Therefore, the key to understanding Bim's role in the apoptotic program is appreciating its relationship to T-cells.

In order to receive stimulatory and growth signals, T-cells need to migrate to environments where these signals are found [4]. An example of one essential signal is the cytokine, interleukin-7 (IL-7). IL-7 is mainly found in generative lymphoid organs as well as some nonlymphoid tissues [5] and is produced in large part by accessory cells [6,7]. The heterodimeric IL-7 receptor (IL-7R), composed of both IL-7Rα and γc chains, is expressed by T-cells [8]. IL-7 is necessary for T-cell development, since disruption of either IL-7 or its receptor resulted in defects in mice [9,10] similar to the SCID (Severe Combined Immunodeficiency Syndrome) phenotype in humans [11]. Evidence of the importance of IL-7 is the fact that excess IL-7 underlies lymphoproliferation and lymphoma formation [12,13], indicating a role in the maintenance of peripheral T-cell homeostasis [14]. IL-7 supports T-cell survival by maintaining a balance between the anti-apoptotic and pro-apoptotic Bcl-2 family members [15,16]. Indicative of a function in T-cell biology, loss of Bim could partially rescue the immunodeficient phenotype of IL-7R$^{-/-}$ mice [17].

How the activity of Bim is regulated remains the focus of study. In some healthy cells, Bim is sequestered by LC8, the light chain element of the microtubule-associated dynein motor complex [18,19] or is bound to anti-apoptotic proteins such as Bcl-2 or Bcl-xL at the mitochondrial interface as was shown in T-cells [20]. Other regulatory mechanisms include transcriptional regulation by FHKR (forkhead) through Foxo3a [21,22], the gastric tumor suppressor, RUNX [23], or the post-translational phosphorylation of Bim at multiple sites [24–30]. We recently showed that IL-7 mediates the phosphorylation of BimEL,

* Corresponding author at: Burnett School of Biomedical Sciences, College of Medicine, University of Central Florida, 6900 Lake Nona Blvd, Orlando, FL 32827, USA. Tel.: +1 407 266 7035; fax: +1 407 266 7003.
E-mail address: annette.khaled@ucf.edu (A.R. Khaled).

0167-4889/$ – see front matter © 2012 Elsevier B.V. All rights reserved.
doi:10.1016/j.bbamcr.2012.06.017

contributing to its pro-apoptotic activity [31]. While a role for Bim as a pro-apoptotic protein is well-recognized, Bim may also have unknown functions that go beyond its described death-promoting activity. Bim exists as multiple isoforms generated through alternative splicing, with the three major isoforms, BimEL, BimL, and BimS, part of a larger cohort of spliced forms [32,33]. Some isoforms lack the BH3 domain or the dynein light-chain binding site, while others lack phosphorylation sites [34], which could result in the possibility that isoforms may have different functions.

When extracellular nutrient sources are limiting, autophagy can support T-cell activation through intracellular scavenging [35], but, under less well-understood conditions, autophagy can also induce T-cell death, for example that of CD4 T-cells [36]. The individual contribution of the major isoforms of Bim to the processes of autophagy or apoptosis in T-cells is unknown. To study this, we used Bim-containing and Bim-deficient T-cells, responsive to IL-7, to examine the activity of the major isoforms in response to the cytokine. A novel role in lysosome positioning was found for BimL that was dependent upon IL-7 and supported the degradative phase of autophagy. In contrast, BimEL and BimS promoted IL-7 withdrawal-induced apoptosis. These results demonstrated that Bim isoforms can participate in distinct apoptotic and lysosomal/degradative activities in T-cells. While Bim has long been recognized as an inducer of apoptosis, its role in supporting lysosome acidification suggests that controlled manipulation of Bim isoforms could lead to novel applications in diseases like cancer.

2. Materials and methods

2.1. Mice, cell lines and culture reagents

C57BL/6 mice were purchased from Jackson Laboratory (Bar Harbor, Maine) and housed at the University of Central Florida, Orlando, FL. Bim knockout (BimKO) mice (C57BL/6 background) [31], $Rag^{-/-}$ and IL-$7^{-/-}$/$Rag^{-/-}$ mice were housed at NCI-Fredrick as previously described [31]. This study was carried out in accordance with the recommendations in the Guide for the Care and Use of Laboratory Animals of the National Institutes of Health. The protocol was approved by the Institutional Animal Care and Use Committee at the University of Central Florida and NCI-Frederick. All efforts were made to minimize suffering.

The IL-7 dependent T-cell line, D1, was established from one clone that arose from T-cells isolated from a $p53^{-/-}$ mouse and immortalized as previously described [37]. Since its establishment in 1997, the D1 cell line has been extensively used to study regulatory pathways controlled by IL-7 in T-cells [16,38–41] and was used to reveal the role of IL-7 in the phosphorylation of BimEL [31]. To uncover the functional consequences of Bim deficiency and evaluate the function of each Bim isoform, we needed a T-cell line that was IL-7 dependent and also Bim deficient. To this end, we generated the SMoR T-cell line. Briefly, lymph node T-cells were isolated from BimKO mice (see above). Cells were resuspended in RPMI 1640, 10% fetal bovine serum (FBS), 5% Penicillin/Streptomyocin (Fisher), 0.1% B-mercaptoethanol (Invitrogen) (complete medium), and 200 ng/ml IL-7 at a concentration of 5×10^5 cells/ml. Using twenty 96-well, round bottom plates, 100 μl or approximately 10^4 cells/well were plated. In total, almost 2×10^7 cells were used for mutagenesis as follows. Ethyl-N-nitrosurea (0.64 mM, ENU) in phosphate/citrate buffer was added to the cultures at 0, 7, 14, 21, and 28 days from initial isolation. Mutagenized T-cells were grown with complete media and IL-7. After 3 months, one BimKO T-cell clone emerged that was immortalized and IL-7-dependent. This outcome recapitulated the same result observed when the original D1 cell line was cloned, in that a single line emerged from the selection process for IL-7 dependency [37]. This experience showed that generating immortalized IL-7 dependent T-cells is not possible unless underlying mutations, such as Bim or p53 deficiency, are present. D1 and SMoR T-cell lines, both derived from mice with a C56BL/6 background, were grown in complete medium and 50–200 ng/ml IL-7. Early passages of D1 and SMoR cell lines were frozen as stocks and cells were used at less than 10 passages from stocks.

Primary lymph node (LN) and splenic T-cells were isolated from both wild-type (WT) and BimKO C57BL/6 mice as previously described [42]. Phoenix cells (see below) were maintained in DMEM medium that was supplemented with 10% FBS.

Reagents used as described in the figure legends include pifithrin-α (p53 inhibitor) (Sigma-Aldrich), 3-methyladenine (3-MA) (class III phosphatidylinositol 3-kinase (PI3K) inhibitor) (Sigma-Aldrich), cathepsin III Inhibitor (pan cathepsin inhibitor, EMD), pepstatin A (cathepsin D inhibitor, EMD) and Ca074 (cathepsin B inhibitor, EMD) and chloroquine (CQ) diphosphate salt (Sigma-Aldrich).

2.2. Viability and proliferation assays

To quantitate cells undergoing apoptosis, the FITC Annexin-V Apoptosis Detection Kit (BD Pharmingen) was used following manufacturer's protocol. This kit utilizes a FITC-conjugated Annexin-V antibody that recognizes phosphatidyl serine exposed on cells undergoing early apoptosis, and contains PI (propidium iodide) which can permeate necrotic, membrane-damaged cells. The Annexin-V/PI kit could not be used with cells expressing GFP (see Section 2.9) as the kit contains a FITC-conjugated antibody whose emissions would overlap the emission of GFP-containing cells. To address this, the SYTOX® AADvanced™ dead cell stain solution and the Violet Ratiometric Membrane Asymmetry Probe/Dead Cell Apoptosis Kit (Invitrogen) was used following the manufacturer's protocol. Apoptosis was indicated by membrane asymmetry using the violet ratiometric dye, and membrane permeability was measured by Sytox uptake. Sytox was visualized at 488 nm and emissions were collected at 695 nm. The violet ratiometric probe was visualized at 405 nm and emissions were collected at 450 nm and 510 nm. Cells were analyzed by flow cytometry using the BD FACSCanto II flow cytometer. Analysis was completed using FCSExpress (DeNovo) software. Viability was also assessed by determining morphological changes, cell shrinkage and granularity, using forward scatter (FSC) and side scatter (SSC) gating by flow cytometry with an Accuri C6 flow cytometer.

Proliferation was measured by labeling cells with CFSE as previously described [42–44]. For CFSE labeling, one million cells were treated with 2 μM CFSE (Molecular Probes) staining solution (PBS + 0.1% BSA) for 10 min and then washed to remove excess label. The division of cells was determined by measuring CFSE fluorescence by flow cytometry after 72 h of culture with or without IL-7. The generation number for the population was determined from a best fit of these data using the proliferation module for the FCS Express software (DeNovo). Unstimulated CFSE-containing cells were used to determine the peak corresponding to the undivided population.

2.3. Bim inhibition by small interfering RNAs

One-to-two million D1 cells were treated with 1–2 nM BCL2L11 SMART pool siRNA (Dharmacon) and Accell delivery media (Dharmacon) supplemented with 1% FBS, and IL-7 (50 ng/ml) for 24 h. After 24 h, cells were deprived of IL-7 and re-plated in media containing the siRNA alone, for 48 h. SMART pool siRNA contains four sequence variations of siRNAs to eliminate non-specific interactions. Non-targeting siRNA (NT siRNA) containing a FAM reporter sequence was used as a delivery control, and was comparable to treatment with Accell media alone. Cells were analyzed using flow cytometry and confocal microscopy.

2.4. Quantitative PCR

Ten million D1 cells, per experimental condition, cultured with or without IL-7 as described above, were re-suspended in 1 ml of TRIzol reagent (Invitrogen). Total RNA was extracted from the cells using the reagent according to the manufacturer's instructions. Each cDNA template

was synthesized from total RNA by reverse transcription with iScript cDNA Synthesis kit according to the manufacturer's instructions. Quantitative analysis of cDNA amplification was assessed by incorporation of SYBR Green (ABI 4385370) into double-stranded DNA. To detect mouse Bim: forward 5′-CGACAGTCTCAGGAGG AACC-3′ and reverse 5′-CCTTCTCCATACCAGA CGGA-3′ primers were used. To detect β-actin as control, forward primer 5′-GAAA TCGTGCGTGACATCAAAG-3′ and reverse primer 5′-TGTAG TTTCATGGATGCCACAG-3′ were used. Reactions contained Fast SYBR Green Master mix (1×), β-actin primers at 50 nM or Bim primers at 100 nM, and 3–4 μg cDNA template. Thermal cycling conditions were as follows: 40 cycles of 30 s at 95 °C followed by 45 s at 57 °C, and 60 s at 72 °C, denaturing, annealing and extension temperatures, respectively. All cDNA samples were processed using the ABI Fast 7500 and analyzed using ABI Sequence Detection Software Version 1.4. The difference in mRNA expression was calculated as follows: RQ value or fold change $= 2^{-\Delta\Delta Ct}$. ΔΔCt is equal to the change in ΔCt values over time after normalization to β-actin. ΔCt is equal to the difference between the endogenous control Ct and target gene Ct values.

2.5. Immunoprecipitation and immunodetection

For preparation of whole cell lysates, 37–45 million cells were lysed using the Cell Lysis buffer (Cell Signaling) in the presence of protease inhibitors (Roche). In the case of primary cells, 1 to 3 million cells per condition, were used. For immunoprecipitation, cell lysates were pre-cleared with Protein A/G Sepharose beads (Santa Cruz), incubated with anti-dynein antibody and immunoblotted for Lamp1 and Rab5 as described below. For immunoblotting, subcellular fractions (from gradients, see Section 2.11), whole cell lysate samples, or co-immunoprecipitated samples were run in 10% or 12–15% SDS-PAGE gels, and proteins were transferred to nitrocellulose membranes by semi-dry transfer (BioRad) or wet transfer (Novex) following the manufacturers' protocols. Membranes were washed and probed with primary antibodies (see below) and incubated with horseradish peroxidase (HRP)-conjugated (Santa Cruz) or fluorescence-conjugated secondary antibodies (LICOR). Signal was detected using either chemiluminescent fempto substrate (SuperSignal West Fempto, ThermoSci) or the LICOR Odyssey detection system. The primary antibodies used in this study were as follows: a rabbit polyclonal antibody against amino acids 22 to 40 of human Bim protein (anti-Bim, Calbiochem), Bim (rat monoclonal 14A8, Calbiochem), Lamp1 (mouse monoclonal 1D4B; developed by J. Thomas August, Developmental Studies Hybridoma Bank, University of Iowa), prohibitin (rabbit polyclonal ab28172, Abcam), p38 (Santa Cruz), Bcl-2 (Santa Cruz), Rab5, an early endosome marker (Abcam), cathepsin B (Abcam), dynein (Abcam), p62 (Cell Signaling), and LC3B (Abcam). Quantitation of the bands was performed using ImageJ software, taking the average of three separate measurements for each band.

2.6. Cell surface protein analysis

Surface expression of IL-7R expressed on T-cells was assessed by flow cytometry using a PE-conjugated anti-IL-7R antibody (BD Biosciences) as previously described [42–44]. A PE-conjugated isotype matched antibody was used as a control for non-specific staining. One–two million D1 or SMoR cells were incubated with or without IL-7 for 18 h and then treated with saturating amounts of the appropriate antibody for 20 min, washed in buffer (PBS + 0.1% BSA) and analyzed by flow cytometry on the Accuri C6 flow cytometer.

2.7. Measurement of intracellular pH

Cells (D1, SMoR, primary C57BL/6 and BimKO) were resuspended in Hanks buffer supplemented with 25 mM HEPES (Invitrogen), 1% FBS, and 1 μM BCECF-AM (Molecular Probes). Intracellular pH-dependent changes in fluorescence were measured by flow cytometry, using methods previously described [45,46]. To establish a pH calibration curve, a separate group of cells (D1, SMoR, primary C57BL/6 and BimKO) was re-suspended in high-potassium HEPES buffer (25 mM HEPES, 145 mM KCl, 0.8 mM MgCl2, 5.5 mM glucose, and DDH2O) at pH standards (5.9, 6.5, 7.0, 7.2, and 7.8) and nigericin (10 μM) was added followed by BCECF-AM. Measurements were acquired using a BD FACSCanto II cytometer excited with a 488 nm laser, with emissions filtered through 525 nm and 610 nm. Dead cells were excluded by forward- and side-scatter gating. pH values were determined by measuring the absorbance ratio between 525 nm (green fluorescence) and 610 nm (red fluorescence), the latter of which compensates for dye concentration, volume, and cell size.

2.8. Live cell imaging/microscopy

For imaging, cells were plated in 24-well glass bottom dishes (MatTek) that had been washed with 1 N HCl and PBS. Cells were treated with 1 μM LysoSensor immediately before imaging. LysoSensor probe is cell membrane permeable and exhibits pH-dependent changes in fluorescence intensity. For imaging of retrovirus-infected cells, dishes were coated with 8 μg/ml Retronectin (Takara), followed by the retroviral supernatant, prior to adding cells. At 20 h post-infection, 1 μM LysoTracker (Molecular Probes) was added to cell culture in RPMI complete media immediately prior to imaging. LysoTracker probes are also cell membrane permeant and contain a fluorophore bound to a weak base that becomes partially protonated upon neutral pH exposure and selectively stains acidic organelles in live cells, although fluorescence is independent of pH changes. Fluorescent images were acquired with the UltraView spinning disk confocal system (PerkinElmer) with AxioObserver.Z1 (Carl Zeiss) stand, and a Plan-Apochromat 40×/1.4 Oil DIC objective. Z-stacks and extended focus of scanned images were created and modified using the Volocity 5.5 image processing program (PerkinElmer). LysoSensor-treated samples were excited at 405 nm. To detect LysoSensor fluorescence, emissions between 445 nm and 615 nm were collected for more neutral pH vesicles (assigned an arbitrary yellow color), and between 525 nm and 640 nm for more acidic vesicles (assigned an arbitrary blue color). LysoTracker stained samples were excited at 561 nm and emissions collected between 525 nm and 640 nm. Transmitted light images were collected for DIC. For SMoR cells expressing pMIG, BimEL, or BimL plasmids, total fluorescence and the number of GFP positive events, with the removal of auto fluorescent outliers, per field, were obtained using Volocity 5.5. GFP was acquired using a 488 nm laser, and emissions were collected at 525 nm and 640 nm.

2.9. Retroviral transfection

The bi-cistronic plasmids, pMIG, pEco, BimEL-pMIG, BimS-pMIG, and BimL-pMIG were made as previously described [31]. The retroviral infection technique was optimized specifically for the D1 and SMoR cell lines [31]. A Phoenix-Eco packaging cell line (Orbigen) was transfected with bi-cistronic plasmids containing a Bim isoform (or none, termed pMIG) and GFP. Cells were transfected using TransIT-LT1 reagent (Mirus). The supernatant containing the retrovirus was harvested after 48 h and loaded onto Retronectin (Takara)-coated plates. 1,000,000 cells/ml were incubated in supplemented media containing Polybrene (Santa Cruz, 8 μg/ml), either in the presence or absence of IL-7, and added to the plates for several hours.

2.10. Adoptive transfer of T-cells and chloroquine in vivo treatment

C57BL/6 and BimKO LN cells were isolated and suspended in PBS containing 5% FBS. Cells were incubated for 10 min with CFSE (Invitrogen) following previously established methods [31]. $Rag^{-/-}$/$IL\text{-}7^{-/-}$ double knockout or $Rag^{-/-}$ recipient mice were irradiated with 3 Gy whole body γ-irradiation 4 h prior to injection. Five million

CFSE-labeled cells were then suspended in PBS and adoptively transferred into the previously irradiated $Rag^{-/-}$, and $Rag^{-/-}$/IL-$7^{-/-}$ double knockout mice. Mice were intraperitoneally injected with 60 mg/kg chloroquine within 24 h, and again, after 48 h. Mice were euthanized within 72 h, spleens and lymph nodes were recovered, and T-cells were isolated and utilized for analysis as previously mentioned [43]. Recovered cells were analyzed for loss of CFSE label by flow cytometry (Accuri C6 flow cytometer) and calculation of generation times was performed using FSC Express (DeNovo) proliferation module software.

2.11. Subcellular fractionation

Cells were seeded to 80–90% confluence. For lysosome preparations: 200 mg (140 million) cells were harvested by isotonic lysis buffer according to protocol from the Lysosome Enrichment Kit (Pierce) and prepared for density gradient ultracentrifugation. Enriched lysosomal fractions were layered onto an iodixanol gradient (17%, 23%, 25%, 27%, 29%, and 30% Optiprep) and subjected to ultracentrifugation using an Optima L-100XP Ultracentrifuge. Fractions from gradients were collected in 500 μl aliquots (fractions 1–10) using an Auto Densi-Flow (Labconco). Enriched preps were utilized for downstream processing or re-suspended in sample buffer for gel-electrophoresis (see below).

2.12. Statistics

Statistical analysis and significance were determined using Prism 5 (Graphpad) for Windows, Version 5.02. P values determined are shown in the figure legends.

3. Results

3.1. Bim has multiple functions, promoting death as well as growth in IL-7 responsive cells

It is generally accepted that Bim inhibits the survival activity of anti-apoptotic members of the Bcl-2 family [47], and that it has an important, although poorly understood, role in T-cell biology [17]. Our previous studies showed that in T-cells, IL-7 regulated the activity of BimEL through phosphorylation [31], but the activity of other major isoforms, BimL and BimS, relative to IL-7 signaling, remained unknown. Using primary LN T-cells from C57BL/6 or BimKO mice, we evaluated the effect of in vitro culture with IL-7, using methods we previously established [42,43]. Shown in Fig. 1A are representative results indicating in the absence of IL-7 that loss of Bim provided short term protection (3 days), although such LN cells eventually died in in vitro culture. Viability of cells was determined by assessing cell shrinkage and increased granularity detected by forward scatter (FSC) and side scatter (SSC) gating using flow cytometry. Because primary T-cells do not uniformly respond to an IL-7 signal (i.e. CD8 T-cells proliferative at the expense of CD4 T-cells) [42,43] and may need additional signals through the T-cell receptor (TCR) for optimal growth [48], we used an IL-7-dependent T-cell line, D1, to examine the activity of Bim in response to IL-7. The generation of the D1 cell line has been previously described [37] and a number of studies have demonstrated its biological relevance in the context of IL-7 signaling [16,38–41,49]. Upon IL-7 withdrawal, cell death, as indicated by increased Annexin-V/PI staining, was detected in D1 cells within 36 h, and death was maximal by 48 h (Fig. 1B) [37]. To determine whether loss of Bim could protect D1 cells from IL-7 deprivation, cells were treated with Bim siRNA, to inhibit total Bim. We observed a 40% reduction in Bim mRNA levels in cells treated with Bim siRNA as compared to cells treated with control siRNA (Fig. 1C). Note that the siRNA methodology limits cell numbers to a few million, which is below the threshold for detection of endogenous Bim protein. The siRNA-induced decrease in Bim expression led to reduced apoptosis in D1 cells deprived of IL-7 as indicated by the increased percentage of viable cells (Annexin-V/PI negative) detected (Fig. 1C). For this experiment, D1 cells were incubated with siRNAs for 72 h, the first 24 h of which was in the presence of IL-7 and the last 48 h was in the absence of IL-7. To determine whether IL-7 regulated the gene expression of Bim, we examined the levels of total Bim mRNA in D1 cells cultured with or without IL-7. Using quantitative PCR, we observed that Bim mRNA levels increased in the absence of IL-7 — specifically after 15–18 h of cytokine withdrawal, indicating that the gene expression of Bim, was in part, IL-7 responsive (Fig. 1D). These results supported the conclusion that Bim was among the effectors of death in response to IL-7 deprivation.

To evaluate the biological consequence of Bim deficiency in IL-7-dependent T-cells and study the function of each major isoform without the limitations imposed by either primary lymphocyte cultures or siRNA treatments, we needed a Bim-deficient and IL-7-dependent T-cell line. To this end, we generated the SMoR T-cell line from BimKO mice as described in Materials and methods. To demonstrate that the expression of Bcl-2 family members in D1 or SMoR cells was not altered by either the immortalization process or loss of p53 or Bim, we examined Bcl-2 and Bax, proteins whose expression or activity, respectively, is regulated by IL-7 [16,37,50]. As shown in Fig. 2A, we found that the two cell lines displayed minimal differences in the amounts of Bcl-2 or Bax detected in response to IL-7. Bcl-2 levels decreased in the absence of IL-7 and Bax distributed between the cytosol and mitochondria (Fig. 2A). Next, we determined whether, lacking functional Bim, SMoR cells underwent death upon IL-7 withdrawal. Apoptosis was detected using Annexin-V/PI staining, and viability was determined by assessing changes in cell size and granularity. Shown in Fig. 2B and C, we observed decreased numbers of Annexin-V/PI positive SMoR cells after 36 h of IL-7 deprivation and sustained viability (50–60%) through 48 h of IL-7 loss. These results indicated that IL-7-dependent, Bim-deficient SMoR cells are useful for the study of Bim function in IL-7 dependent T-cells and confirmed that Bim was contributing to death induced by IL-7 loss.

As shown and previously reported, D1 cells underwent death between 24 and 48 h after IL-7 withdrawal (Fig. 2C) [37]. Stimuli that induce apoptosis can also trigger DNA damage and p53 is usually responsive to this mechanism [51]. To show that protection from IL-7-withdrawal-induced death in SMoR cells was likely due to loss of Bim and not the presence of a possible p53-mediated activity, we treated cells with pifithrin-α, originally described as a p53 inhibitor [52], but also shown to protect from DNA-damage induced apoptosis [53]. No differences in the viability of SMoR cells or D1 cells, cultured with IL-7, were detected upon pifithrin treatment (Supplemental Fig. 1). Withdrawal of IL-7 and the addition of pifithrin increased the death observed in D1 cells, suggesting that both p53-dependent and p53-independent death mechanisms were involved. In contrast, SMoR cells were resistant to death induced by increasing doses of pifithrin-α (Supplemental Fig. 1), indicating that the loss of Bim was likely a key factor that contributed to protective effect observed upon IL-7 withdrawal (Fig. 2C). Note that upon extended IL-7 deprivation, SMoR cells eventually died after 4 days (data not shown). Hence, the loss of Bim did not prevent but delayed the death of cells deprived of IL-7.

Other parameters of importance are cytokine-driven proliferation and viability under conditions of nutrient deprivation. To measure the growth of D1 and SMoR cells in response to IL-7, we used the dye, CFSE. CFSE divides with each cell replication cycle and can be used to measure generation times as shown in Fig. 2D. D1 cells rapidly divided in response to IL-7, replicating 1–2 times per day over the three days of evaluation, while SMoR cells divided 1–2 times over the same three day period (Fig. 2D). Therefore, loss of Bim, while providing protection from IL-7-induced cell death (Fig. 2C), decreased cell replication rate. The surface expression of the IL-7R was measured to

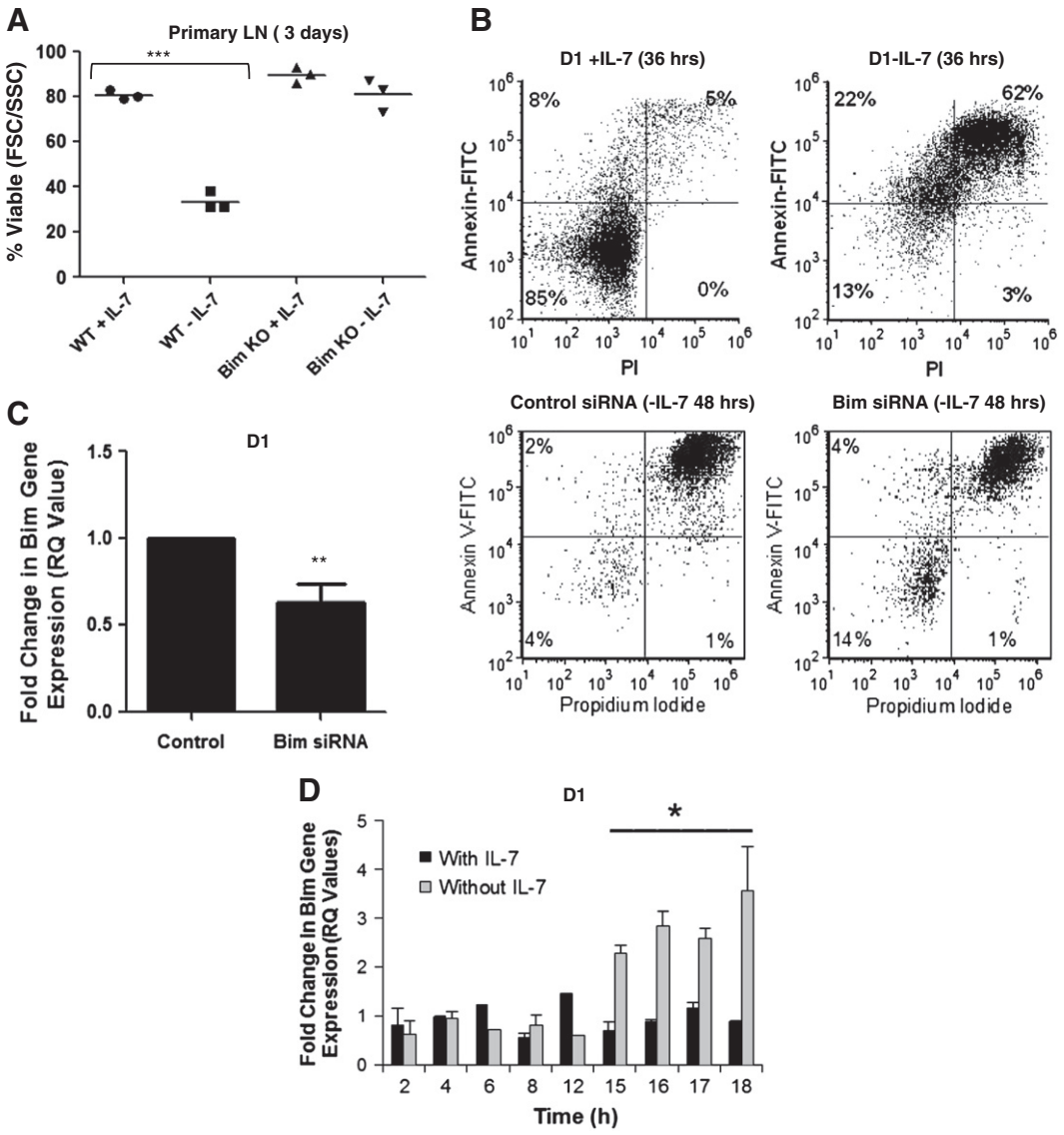

Fig. 1. Loss of Bim partially protects IL-7 dependent cells from apoptosis. (A) Lymph node T-cells, isolated from WT C57BL/6 or BimKO mice and cultured with or without 150 ng/ml of IL-7 for 3 days as described in Materials and methods, were assessed for viability as determined by cell morphology, assessing size (forward scatter (FSC)) and granularity (side scatter (SSC)) by flow cytometry. (B) Cytokine withdrawal-induced death of D1 cells, grown with or without 50 ng/ml IL-7 (36 h), was measured by surface expression of phosphatidyl serine using FITC-conjugated Annexin-V antibody. Membrane permeability was assessed by propidium iodide exclusion (PI), analyzed by flow cytometry. Dot plots show percentages representing the population of cells that are non-apoptotic (lower left quadrant), early apoptotic (upper left quadrant) or late apoptotic/necrotic (upper right quadrant). Quadrants were established using controls. (C) D1 cells were pre-treated with non-targeting control or BCL2L11 SMART pool siRNA (Dharmacon) for 24 h with IL-7. Cells were then deprived of IL-7 for 48 h. Efficacy of Bim siRNA upon Bim mRNA levels (graph) was established by measuring total Bim gene expression by quantitative PCR in which RQ value (or fold change in gene expression) $= 2^{-\Delta\Delta Ct}$. IL-7-withdrawal-induced death in D1 cells, treated with either non-targeting control (control) or Bim siRNA, is shown (dot plots) using Annexin-V/PI staining as described above. (D) Total Bim gene expression in D1 cells, in the presence or absence of IL-7, was measured for the times indicated by quantitative PCR. RQ (Fold change) $= 2^{-\Delta\Delta Ct}$. Data shown in this figure are representative of a minimum of three independent experiments. * $P<0.05$, ** $P<0.0241$, *** $P<0.0001$.

determine whether the slow growth of SMoR cells was due to decreased IL-7R levels. This was not observed, as is shown in Fig. 2E. Both D1 and SMoR cells displayed comparable levels of IL-7R that increased upon cytokine withdrawal, a pattern that is typical of what others have reported [54]. In fact, compared to D1 cells, SMoR cells had slightly higher amounts of surface IL-7R relative to maximal receptor levels achieved in the absence of IL-7 (Fig. 2E). SMoR cells, but not D1 cells, were also more sensitive to glucose deprivation and decreased viability when cultured under conditions of minimal glucose (4 mM) (Fig. 2F). These results suggested that loss of Bim conferred partial protection from cell death caused by growth factor removal but also caused a growth disadvantage that resulted in reduced replication and sensitivity to nutrient loss that was not dependent on the levels of IL-7R.

3.2. Bim supports intracellular acidification and formation of acidic vesicles

In order to investigate the activity of Bim in IL-7 dependent T-cells that could account for the observed biological effects, changes in intracellular pH were examined. Cytosolic acidification can be a hallmark of apoptosis and has been linked with lysosomal proton release upon lysosomal permeabilization [55,56]. Changes in pH can also correlate with proliferative status [57]. A time course experiment, measuring intracellular pH, showed that D1 cells acidify after 24–30 h of IL-7 withdrawal, consistent with morphological changes that are indicative of cell death (Fig. 3A). In SMoR cells, IL-7 deprivation did not induce acidification and cells remained more alkaline over the entire course of evaluation (Fig. 3A). These results were confirmed using

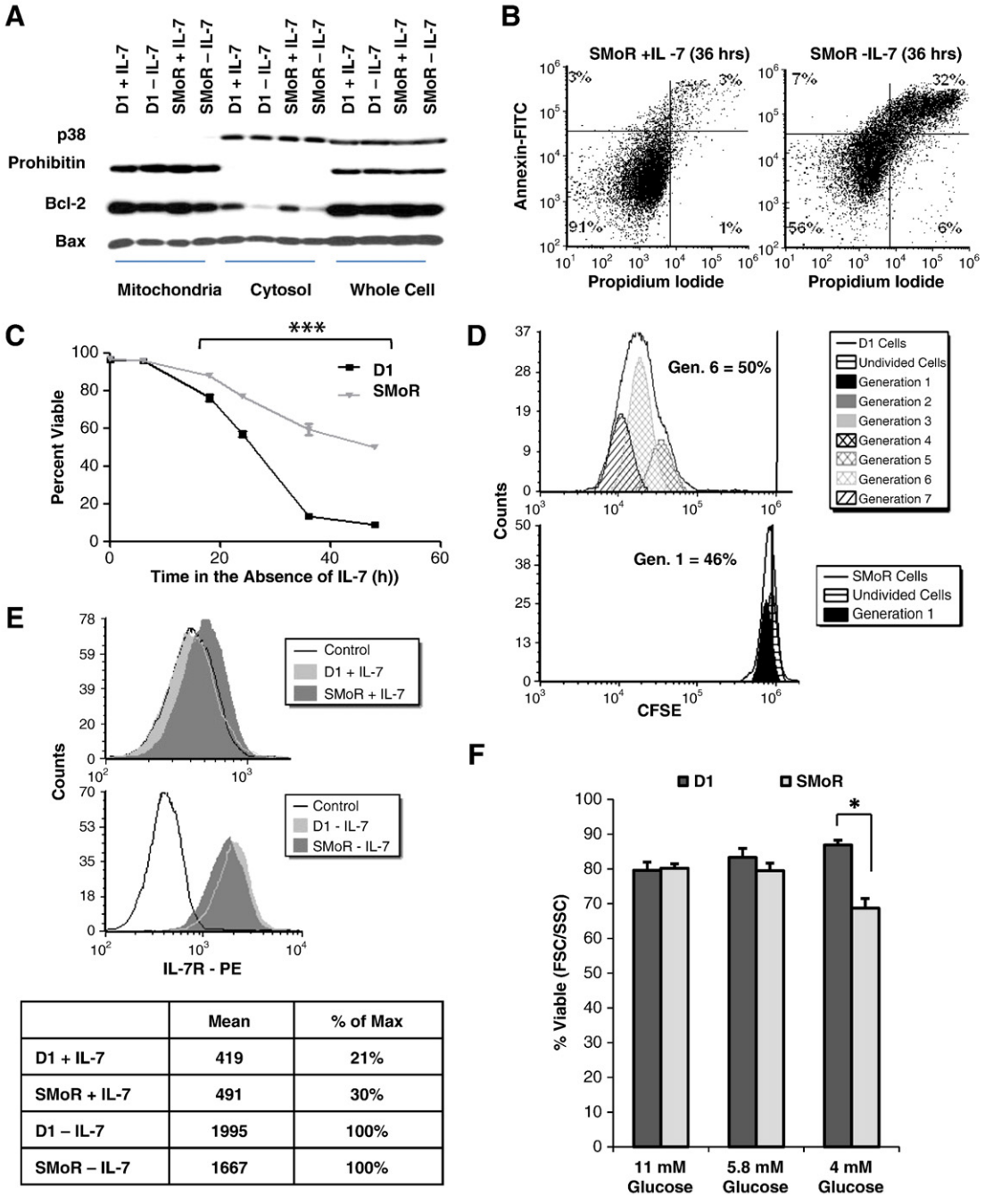

	Mean	% of Max
D1 + IL-7	419	21%
SMoR + IL-7	491	30%
D1 – IL-7	1995	100%
SMoR – IL-7	1667	100%

Fig. 2. Characterization of SMoR cells. (A) Expression of Bcl-2 and Bax in D1 and SMoR cells, cultured with or without IL-7 for 18 h, was examined by immunoblot. Prohibitin and p38 MAPK are shown as loading controls for mitochondrial and cytosolic content, respectively. (B) Cytokine-withdrawal-induced death of SMoR cells, grown with or without IL-7 (36 h), was measured using FITC-conjugated Annexin-V antibody and PI as previously described. (C) Viability of D1 and SMoR cell lines, without IL-7 for the hours indicated, was determined by assessing morphological changes using FSC and SSC gating as previously described. (D) CFSE labeled D1 and SMoR cells were cultured with IL-7 for 72 h. Generation or doubling time, as indicated by loss of CFSE label, was assessed by flow cytometry as described in Materials and methods. Histograms display the fluorescence profile of CFSE-labeled cells analyzed using FCS Express Proliferation software (DeNovo). The percent of cells in the peak generation for each cell line is shown. Lines indicate undivided cells and peaks indicate divided cells. Tables at the far right display the number of generations within the experimental period for each cell line. (E) Histograms show the surface expression of IL-7R in D1 and SMoR cells in the presence or absence of IL-7 for 18 h, using a specific PE-conjugated anti-IL-7 antibody, analyzed by flow cytometry. Table shows the mean for each peak and the percent of IL-7R expression compared to the maximum level achieved in the absence of IL-7. (F) D1 and SMoR cells were cultured in the presence of IL-7 and limiting concentrations of glucose for 114 h. Viability was determined by cell morphology, assessing size (forward scatter (FSC)) and granularity (side scatter (SSC)) by flow cytometry. Results shown are representative of three experiments. * $P<0.05$, *** $P<0.0001$.

LN T-cells from WT and BimKO mice (Fig. 3B). While we previously showed that D1 cells transiently alkalinize 6–8 h after IL-7 withdrawal due to the activity of the sodium hydrogen exchanger 1 (NHE1) [16], this is an active mechanism induced by apoptotic stimulus [45]. In contrast, the increased intracellular pH of SMoR cells was detectable in the presence of IL-7 and did not change even during IL-7 withdrawal.

These data suggested that Bim loss was affecting a biological activity that impacted upon intracellular pH. One possibility could be that the loss of Bim disrupted normal lysosomal functioning. To determine whether the morphology of lysosomes was different in Bim-containing and Bim-deficient cells, endosomes and lysosomes were visualized using the LysoSensor probe. LysoSensor measures the pH of acidic organelles and

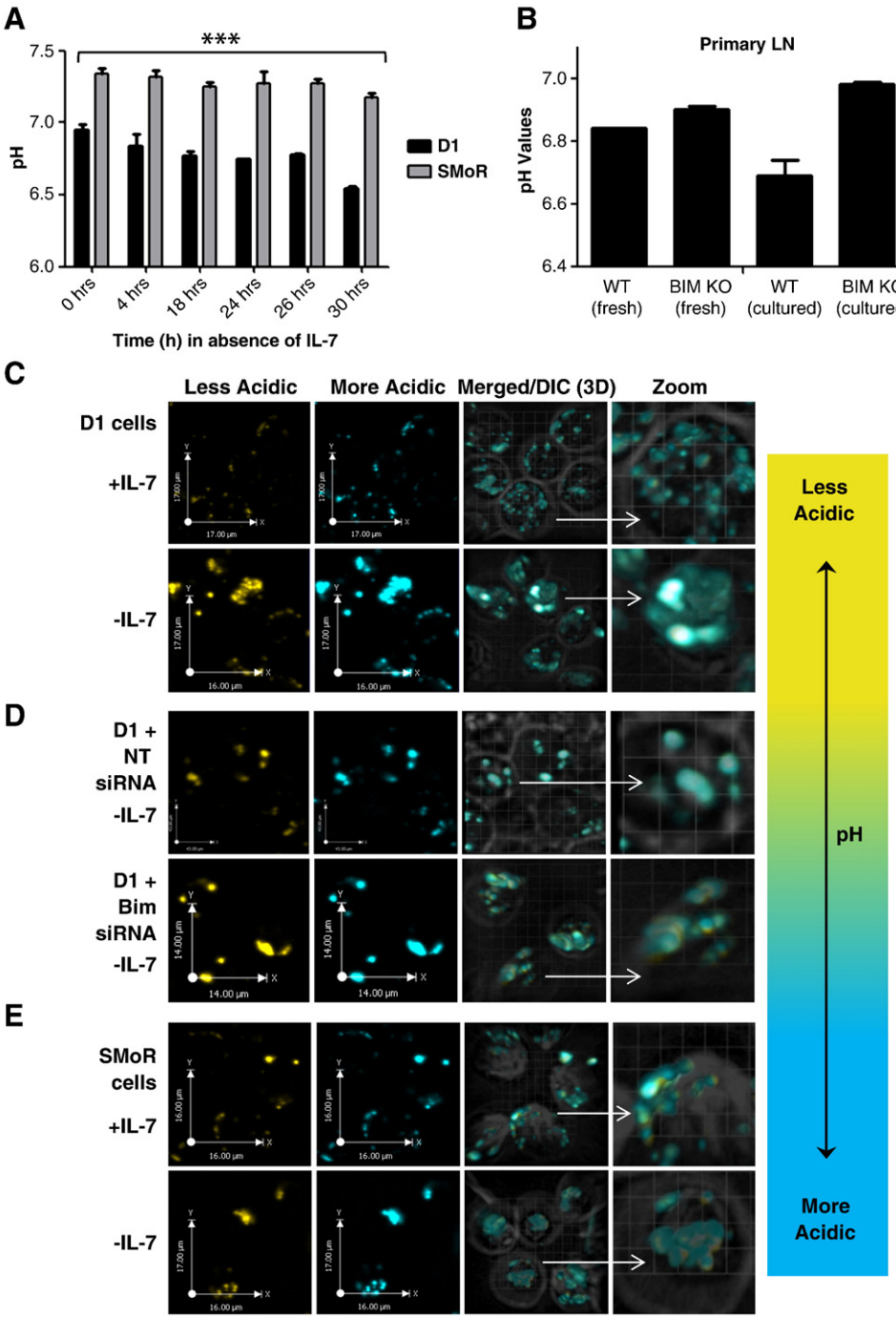

Fig. 3. The distribution of acidic vesicles is altered in absence of Bim. (A) Intracellular pH of D1 and SMoR cell lines was measured in the absence of IL-7 at times indicated in the figure using flow cytometric analysis of BCECF-AM fluorescence, assessing the ratio at 525 nm and 610 nm. Results were determined from calibrated pH standards as described in Materials and methods. (B) Lymph node T-cells isolated from WT C57BL/6 or BimKO mice, either freshly isolated (fresh) or cultured with 150 ng/ml of IL-7 (cultured) for 4 days, were assessed for pH, as determined by flow cytometric analysis of BCECF-AM fluorescence described above. (C–E) Live cell confocal microscopy images of D1 cells (C) in the presence or absence of IL-7 for 20 h are shown. Cells were loaded with LysoSensor as described in Materials and methods. IL-7-deprived D1 cells, containing either non-targeting control (NT) or Bim siRNA (D), were loaded with LysoSensor and imaged as described above. SMoR cells (E) grown with or without IL-7 were loaded with LysoSensor and imaged as described above. Yellow color indicates fluorescence of intracellular vesicles at a more neutral pH acquired at emissions 445/615, and blue color indicates fluorescence of vesicles at acidic pH acquired at 525/640 nm. Colors were arbitrarily chosen. Fluorescent images were obtained using the UltraView spinning disk confocal system (PerkinElmer) with AxioObserver.Z1 (Carl Zeiss) stand, and a Plan-Apochromat 40×/1.4 Oil DIC objective. For (C–E), images were obtained from Z-series collections and 3D projections developed using Velocity software. Arrows indicate regions of interest or intensity/merged vesicle staining. Images are representative "snapshots" of three or more independent experiments. ***$P<0.001$.

distinguishes more neutral vesicles of higher pH (i.e. endosomes) from acidic or lower pH vesicles (i.e. late endosomes/lysosomes). In parallel studies, the probe LysoTracker was used to visualize lysosomal content and show that no pH-dependent changes in the probe occurred in the organelles imaged, demonstrating that LysoTracker staining and LysoSensor staining were comparable (Supplemental Fig. 2). Live cell imaging was

performed to view results from lysosome probes. In Fig. 3C, using LysoSensor, we observed a difference in the distribution and aggregation of less acidic (arbitrarily assigned a yellow color) compared to more acidic vesicles (arbitrarily assigned a blue color) in D1 cells grown with or without IL-7. The dispersed distribution of acidic vesicles within cells cultured with IL-7 became clumped and aggregated as IL-7 was deprived, indicating a potential increase in endosome/lysosome fusion. This is best observed in the 3-dimensional (3D) single-cell enlargement showing intense staining of merged fluorescent signals (appearing white in areas) from acidic vesicles (Fig. 3C). When D1 cells were treated with Bim siRNA, a distinct change was observed in that aggregation was decreased (no intense staining of merged fluorescence or white areas) and increased detection of less acidic vesicles (Fig. 3D). This is most clearly seen in the merged 3D enlargement. These results suggested that loss of Bim had a negative effect upon the distribution of acidic vesicles. This was confirmed in SMoR cells with increased detection of less acidic vesicles (Fig. 3E) in the presence or absence of IL-7. In total, increased intracellular alkalinity and decreased acidic vesicles in Bim deficient cells suggested that Bim could have a function in the maintenance of lysosomal activity.

3.3. The absence of Bim leads to impairment of the later degradative phase of autophagy

Our data showing that SMoR cells lacking Bim were less viable under conditions of limiting glucose (Fig. 2F) and has less acidic vesicles (Fig. 3E), suggested that Bim could be involved in a novel biological activity, that of self-eating or autophagy. Autophagic digestion can contribute to the recycling of cytoplasmic components and promote survival, the inhibition of which may enhance apoptosis [58]. Alternatively, autophagy can directly lead to cell death [59]. To examine this, we used the class III PI3K inhibitor, 3-MA, which can inhibit autophagy under conditions of nutrient or cytokine deprivation [60]. We observed that 3-MA treatment accelerated cell death in the absence of IL-7 — from 32% (untreated) to 49% (3-MA) apoptotic/necrotic cells (Fig. 4). Treatment with 3-MA had only a minor impact in Bim deficient SMoR cells and did not greatly increase the percent of apoptotic/necrotic cells — from 8% (untreated) to 12% (3-MA) (Fig. 4). We also observed that treatment with 3-MA caused some death in the presence of IL-7 (Fig. 4), which could be due to the effect of this inhibitor on PI3 Kinases [60].

To assess autophagic activity, the levels of LC3-I and LC3-II were measured. LC3-I is cytosolic, while LC3-II, which is conjugated with phosphatidylethanolamine (PE), is associated with autophagosomes and less so with autolysosomes [61,62]. Normally the amount of LC3-II correlates with the number of autophagosomes and is degraded as a result of autophagy. As shown in the representative experiment in Fig. 5A, LC3-I and LC3-II levels varied slightly in D1 cells cultured with IL-7 for 6 or 18 h, with more LC3-I and less LC3-II detected at 18 h. In contrast, D1 cells deprived of IL-7 for 6 h (or at 18 h) had an increased ratio of LC3-II to LC3-I, suggesting an increased number of autophagosomes (Fig. 5A). In comparison, SMoR cells displayed higher amounts of both LC3-I and LC3-II, suggesting that either autophagosomes were increased in these cells or that degradation of LC3 was reduced, allowing the protein to accumulate (Fig. 5A). Note that by 18 h of IL-7 deprivation, levels of LC3-I and II were negligible in both D1 and SMoR cells. Next, we examined the degradation of p62 (a.k.a. SQSTM1) as an indicator of autophagic flux. The targeting of p62 to the autophagosome formation site does not require LC3, however, once there, p62 binds to LC3 and is entrapped in autophagosomes where, upon fusion with lysosomes, it is degraded [63]. Hence, impairment of the degradative phase of autophagy can result in the accumulation of p62. We observed that in D1 cells, the levels of p62 declined when IL-7 was withdrawn, suggestive of increased autophagic degradation (Fig. 5A). This did not occur in SMoR cells where p62 levels remained elevated (Fig. 5A). We confirmed these results using freshly isolated LN T-cells from BimKO and WT mice. In

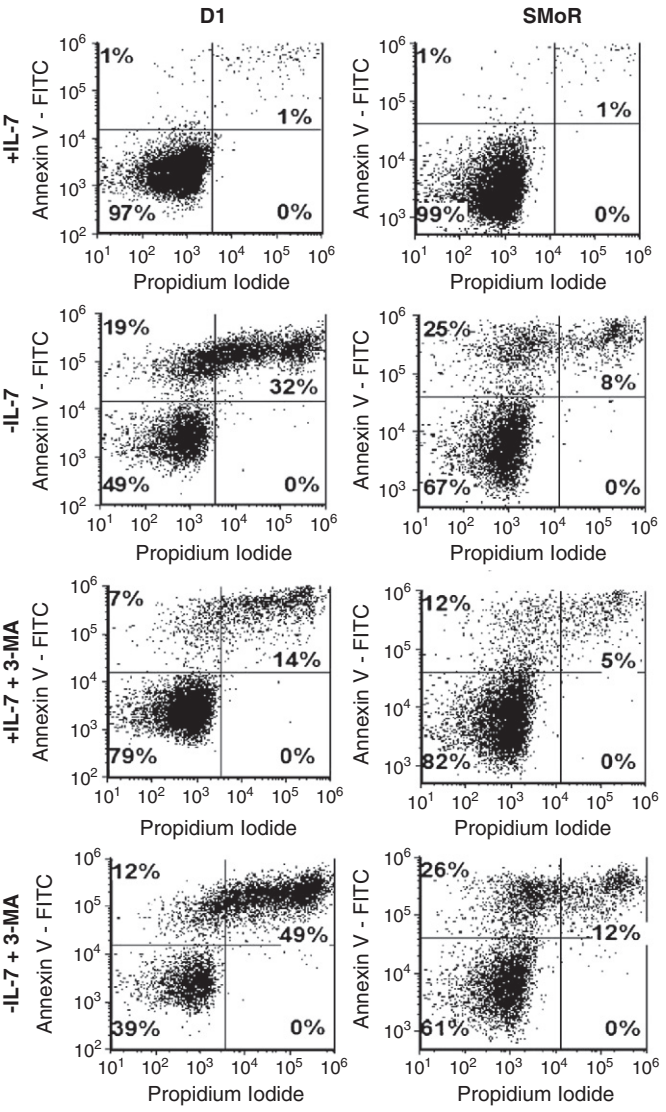

Fig. 4. Treatment with 3-MA accelerated cell death induced by IL-7 withdrawal but not in Bim deficient cells. D1 and SMoR cells, cultured with or without IL-7 for 18 h, were treated with 3-MA (5 mM) as described in Materials and methods. Cell death was assessed by measuring phosphatidyl serine surface exposure and membrane permeability with a FITC-conjugated Annexin-V antibody and PI staining using flow cytometry. Dot plots show percentages representing the population of cells that are non-apoptotic (lower right quadrant), early apoptotic (upper right quadrant) or late apoptotic/necrotic (upper left quadrant). Quadrants were established using controls. Results shown are representative of four independent assays.

comparison to WT cell, we detected elevated levels of LC3-II compared to LC3-I in BimKO cells, with a greatly increased ratio of LC3-II to LC3-I and increased accumulation of p62 (Fig. 5B). This data suggested that loss of Bim did not impair autophagosome formation, since LC3-II and p62 were detected, but could suggest a problem with the degradative phase of autophagy that allowed these proteins to accumulate.

To study lysosomal-mediated degradative activity, we used the inhibitor, chloroquine (CQ), to inhibit lysosomal acidification. As a comparison, we also used 3-MA. Within the timeframe of the experiment with freshly isolated LN cells, these inhibitors did not greatly impact upon LC3 and p62 protein levels (Fig. 5B). However, inhibition of lysosomal acidification with CQ did increase LC3-II accumulation in D1 cells grown with or without IL-7 (Fig. 5C) and also increased the amount of p62 (Fig. 5D), indicating that these proteins were being degraded as a result of lysosomal activity. Treatment with 3-MA had a similar, though slightly lesser, effect (Fig. 5C–D). This suggested that

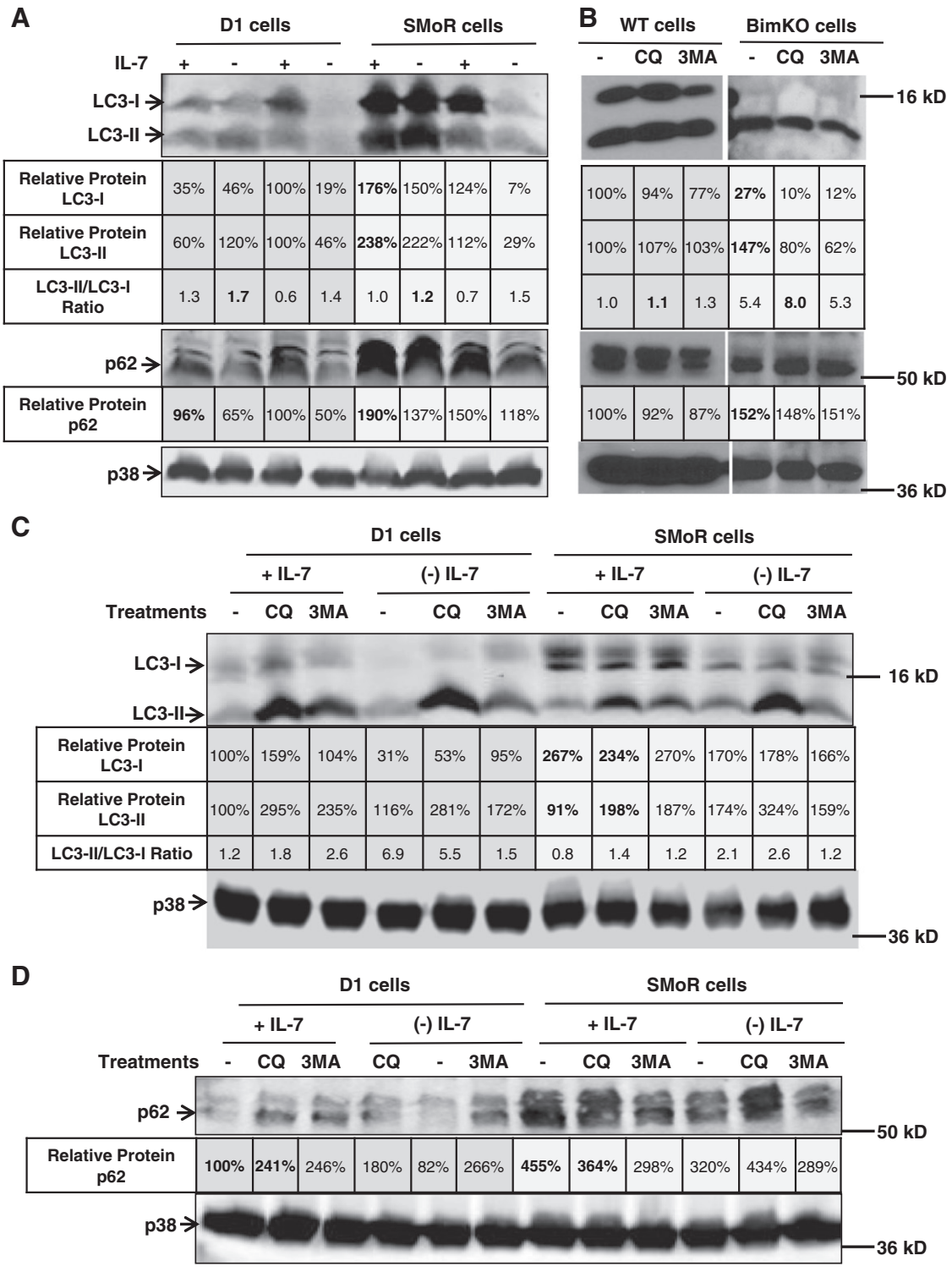

Fig. 5. The degradative phase of autophagy is impaired by Bim loss. (A) D1 and SMoR cells were grown with or without IL-7 for 6 or 18 h, and whole cell lysates were prepared as described in Materials and methods. Lysates were immunoblotted with specific antibodies for LC3 to examine levels of LC3-I and LC3-II as well as p62. Quantitation of bands was performed using Image J software and is the average of 3 measurements taken per band. p38 MAPK is included as a loading control. Protein levels of LC3 and p62 were normalized to p38 MAPK and percentages of protein detected are shown relative to samples from D1 cells cultured 18 h with IL-7. Results shown are representative of three independent experiments. (B) Whole cell lysates were prepared from primary LN cells freshly isolated from WT and BimKO mice and immunoblotted for LC3 and p62 as described above. Cells were treated with 3-MA (5 mM) or chloroquine (CQ) (25 μM) for 6 h prior to lysis. p38 MAPK is shown as a loading control and quantitation of bands was performed as described in (A) with percentages of protein shown relative to untreated WT cells. (C–D) D1 and SMoR cells were cultured with or without IL-7 for 6 h and treated with 3-MA or CQ as described above. Lysates were immunoblotted for LC3 (C) and p62 (D) following protocols described above. p38 MAPK is shown as a loading control for each blot and quantitation of bands was determined as described in (A) with percentages of proteins shown relative to D1 cells untreated and cultured with IL-7. Results are representative of three independent experiments. Images from full-length blots were cropped for concise presentation.

in Bim-containing D1 cells, autophagosome formation was occurring, followed by autolysosomal-mediated protein degradation. In SMoR cells CQ treatment also caused some accumulation of LC3-II but to a lesser extent than in D1 cells (Fig. 5C). As example, in D1 cells cultured with IL-7, CQ treatment caused an almost three-fold increase in LC3-II as compared to SMoR cells in which a slightly more than two-fold increase

was observed (Fig. 5C). Note also that in SMoR cells, higher levels of LC3-I were found that resulted in lower ratios of LC3-II to LC3-I. The amount of p62 protein was also elevated in SMoR cells and was not significantly increased by CQ or 3-MA treatments (Fig. 5D). These results supported the idea that Bim is needed to enable the degradative phase of autophagy, impairment of which could have a negative feedback upon the initiation of autophagy and LC3 conversion levels.

To strengthen the conclusion that the lysosomal/degradative phase of autophagy is defective in Bim-deficient cells, SMoR cells were treated with inhibitors of cathepsin activity or lysosomal

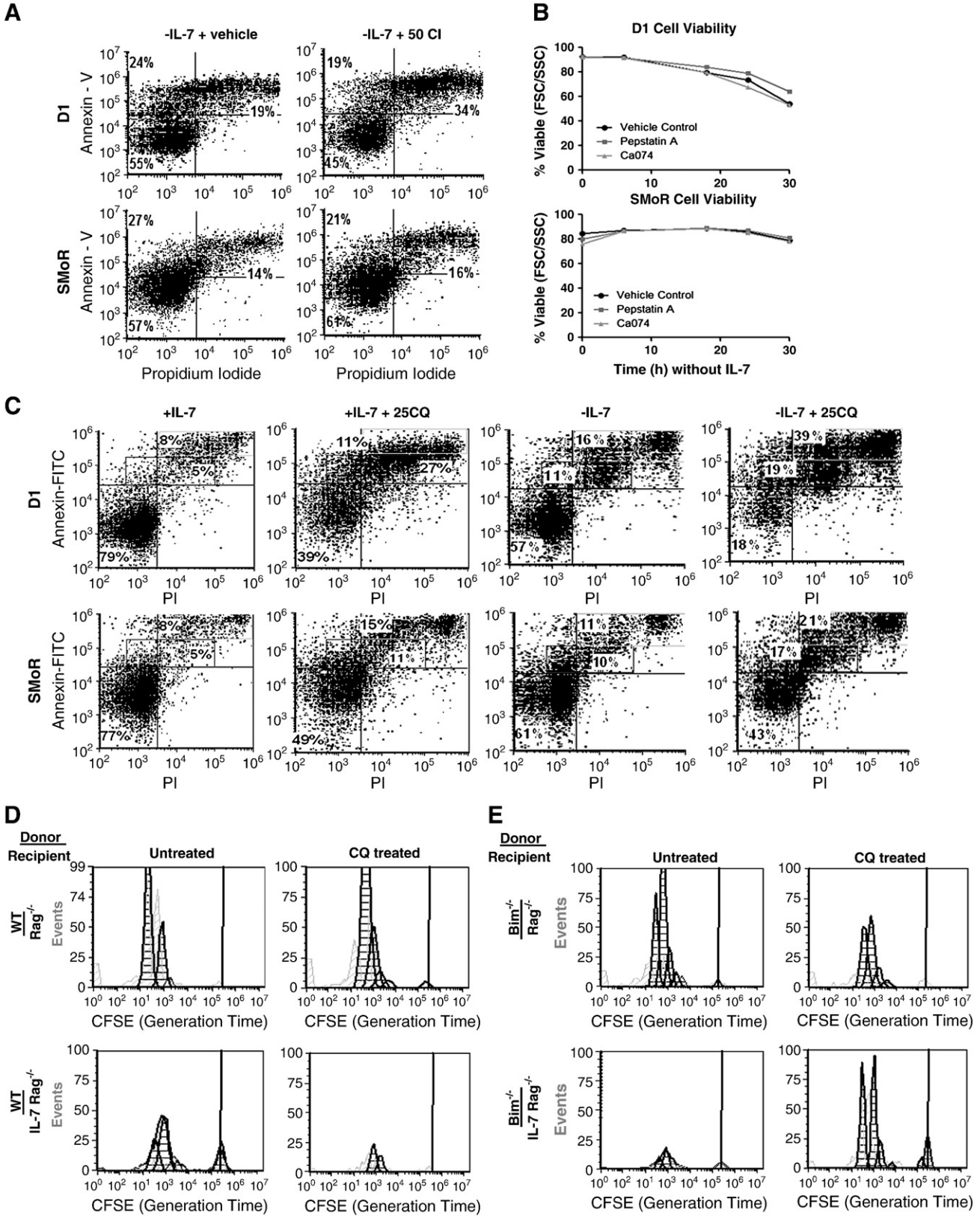

acidification. The expectation was that Bim deficiency would render SMoR cells resistant to the effect of these inhibitors. In Fig. 6A, a representative experiment with SMoR cells is shown in which treatments with a pan-cathepsin inhibitor (CI) had little effect on IL-7-withdrawal induced apoptosis. Results were confirmed with specific inhibitors of aspartic proteases, like cathepsin D (pepstatin A) and cathepsin B (Ca074) (Fig. 6B). With the autophagy process intact, D1 cells showed the anticipated effect of accelerated cell death upon CI (Fig. 5A) and pepstatin A (Fig. 5B) treatments. Note that inhibitors of specific cathepsins were less effective than the pan-cathepsin inhibitor (CI), likely because the specific cathepsins inhibited were less active in these cells. To further examine the effect of Bim upon the lysosomal activity, CQ was used [64]. CQ is being tested as a therapeutic agent and is well-tolerated at treatment doses [65]. A CQ dose–response curve was experimentally determined (data not shown). The representative experiment in Fig. 6C revealed that in the presence of IL-7, CQ caused less death in SMoR cells, and, upon IL-7 withdrawal, SMoR cells were resistant to the effects of CQ and did not accumulate large numbers of late-apoptotic/necrotic cells. As expected, Bim-containing, D1 cells underwent accelerated IL-7-induced apoptosis upon CQ treatment, with increased amounts of apoptotic/necrotic cells detected, as measured by Annexin-V/PI staining (Fig. 6C). These results suggested that the autophagy defect in Bim-deficient cells might be associated with the formation of degradative autolysosomes. Findings in Fig. 3, that SMoR cells were more alkaline and accumulated fewer acidic vesicles provide additional support for this idea.

Studies performed with T-cell lines were extended to mice to determine whether inhibition of lysosome acidification accelerated the death of WT, but not BimKO, T-cells adoptively transferred to $Rag^{-/-}IL\text{-}7^{-/-}$ mice. Recipient $Rag^{-/-}$ (control) or $Rag^{-/-}IL\text{-}7^{-/-}$ mice were treated with CQ as described in Materials and methods, and splenic CFSE-labeled T-cells were recovered for analysis. Generation or doubling time was determined by the number of cycles in which the CFSE label was halved during each cell division. Results are shown in Fig. 6D–E. We observed that WT T-cells transferred to control $Rag^{-/-}$ mice proliferated equally well in the absence or presence of CQ (Fig. 6D). The same was true with BimKO T-cells, although the total cell number was slightly reduced during CQ treatment (Fig. 6E). When WT cells were transferred to $Rag^{-/-}IL\text{-}7^{-/-}$ mice, proliferation was greatly reduced and a significant number of cells remained undivided (Fig. 6D). Moreover, loss of Bim did not rescue T-cell expansion in the absence of IL-7 (Fig. 6E). However, CQ treatment did complement Bim deficiency and restored T-cell growth in mice lacking IL-7 (Fig. 6E). Note that we observed a similar finding in that SMoR cells were more resistant to CQ treatment (Fig. 6C). CQ treated WT T-cells transferred to $Rag^{-/-}IL\text{-}7^{-/-}$ mice did not proliferate and fewer cells were recovered than was observed for untreated WT cells under IL-7-deficient conditions (Fig. 6D). These results confirmed the in vitro results described for T-cell lines (Fig. 6C) that inhibition of lysosomal activity can accelerate death during an apoptotic stimulus, like IL-7 withdrawal, and that this does not occur in cells lacking Bim.

3.4. Bim isoforms differentially contribute to apoptotic and lysosomal activities

The results obtained indicated that Bim could have possible roles supporting both apoptosis and the degradative, lysosomal-mediated phase of autophagy. The question remained — how can Bim function in both capacities? A possible answer could be that Bim isoforms have different roles in these processes. To determine this, we examined the expression of the major isoforms of Bim in response to IL-7. To localize the major Bim isoforms, BimEL, BimL and BimS, to organelles, density gradient separation of cell lysates was performed. This procedure allows the separation of organelles and membrane-encased vesicles based upon lipid and protein content. In Fig. 7A, a representative experiment shows that in Bim-containing D1 cells, cultured with IL-7, we detected BimL protein in fraction 3 that is associated with late endosomes/lysosomes and marked by the highest concentration of Lamp1 (fractions 1–4). Note that Lamp1 is diagnostic for lysosomal-associated disorders [66] and thus a marker for lysosome content. A small amount of the early endosome marker, Rab5, also associated with the same fraction. As a control, we observed that Bcl-2 associated with those fractions in which prohibitin, a mitochondrial marker, was found (fractions 3–5, but highest in fraction 4) as well as small amounts of the other major Bim isoforms (Fig. 7A).

Performing gradient centrifugation using cell lysates from IL-7-deprived D1 cells, we detected increased amounts of BimEL and BimS that associated with mitochondrial fractions marked by Bcl-2 and prohibitin (fractions 3–6, but mostly in fraction 4) and decreased amounts of BimL that associated with lysosomes (Fig. 7A). Interestingly, more BimEL was seen across fractions 1–5, while BimL and BimS were concentrated in the mitochondrial-associated fractions. We also observed an increase in Lamp1 staining in the lightest density fraction (fraction 1) and a weak but dispersed distribution of Rab5. These results demonstrated that the isoforms of Bim could localize to different organelles based on the lipid/protein content in the presence of IL-7 as compared to the absence of IL-7. Significantly, we found that BimL was associated with lysosome fractions in the presence of IL-7.

In Fig. 7B, similar density gradient experiments performed with SMoR cells are shown. Overall Lamp1 levels were reduced in the lighter density fractions (fraction 3 in the presence of IL-7 and fraction 1 in the absence of IL-7). While Lamp1 staining was decreased, Rab5 staining was increased, which supported the imaging experiments in Fig. 3 and suggested that early endosomes (or more neutral vesicles) were more abundant in the absence of Bim. Like in D1 cells, Bcl-2 in SMoR cells was mainly associated with mitochondrial fractions (Fig. 7B). Note that SMoR cells, like freshly isolated BimKO LN and spleen cells (see Supplemental Fig. 3), express polypeptides that migrate in a gel at the same levels of endogenous BimL and BimS.

The results shown indicated that BimL may directly associate with lysosomes in IL-7 cultured cells. This could occur through association with the microtubule motor, dynein. Previous studies had shown an interaction between Bim and dynein that sequestered that BH3-only

Fig. 6. Bim deficient cells are resistant to inhibition of lysosomal activity. (A) Cytokine-withdrawal induced death of D1 and SMoR cells cultured without IL-7 and either DMSO (vehicle control) or 50 μM pan-cathepsin inhibitor (cathepsin inhibitor III (CI)) was measured by surface expression of phosphatidyl serine using a FITC-conjugated Annexin-V antibody. Membrane permeability was assessed by propidium iodide exclusion (PI) and analyzed by flow cytometry. Dot plots show percentages representing the population of cells that are non-apoptotic (lower left quadrant), early apoptotic (upper left quadrant) or late apoptotic/necrotic (upper right quadrant). Quadrants were established using controls. (B) D1 and SMoR cells cultured without IL-7 and either DMSO (vehicle control), 5 μM pepstatin A (cathepsin D inhibitor), or 10 μM Ca074 (cathepsin B inhibitor) for times indicated, were assessed for viability as determined by cell morphology, assessing size (forward scatter (FSC)) and granularity (side scatter (SSC)) by flow cytometry. (C) D1 and SMoR cells cultured with IL-7 or without IL-7 and 25 μM chloroquine (25CQ) were assayed for Annexin-V/PI staining by flow cytometry as described above. Percentages shown represent the population of cells indicated by the highlighted boxes of late apoptotic or necrotic cells. Results shown are representative of four experiments. (D–E) CFSE-labeled T-cells were adoptively transferred to either Rag knockout ($Rag^{-/-}$) or IL-7/Rag double knockout ($IL\text{-}7^{-/-}/Rag^{-/-}$) that were irradiated as described in Materials and methods. Mice were untreated or treated with chloroquine (CQ) (i.p. 60 mg/kg/mouse) 24 and 48 h after transfer of cells. Mice were sacrificed after 72 h and organs were analyzed for T-cell recovery. The number of generations recovered from transferred WT cells (D) and BimKO cells (E) was determined by loss of CFSE label using cell proliferation software (FCS Express, DeNovo). Representative results from duplicate experiments are shown.

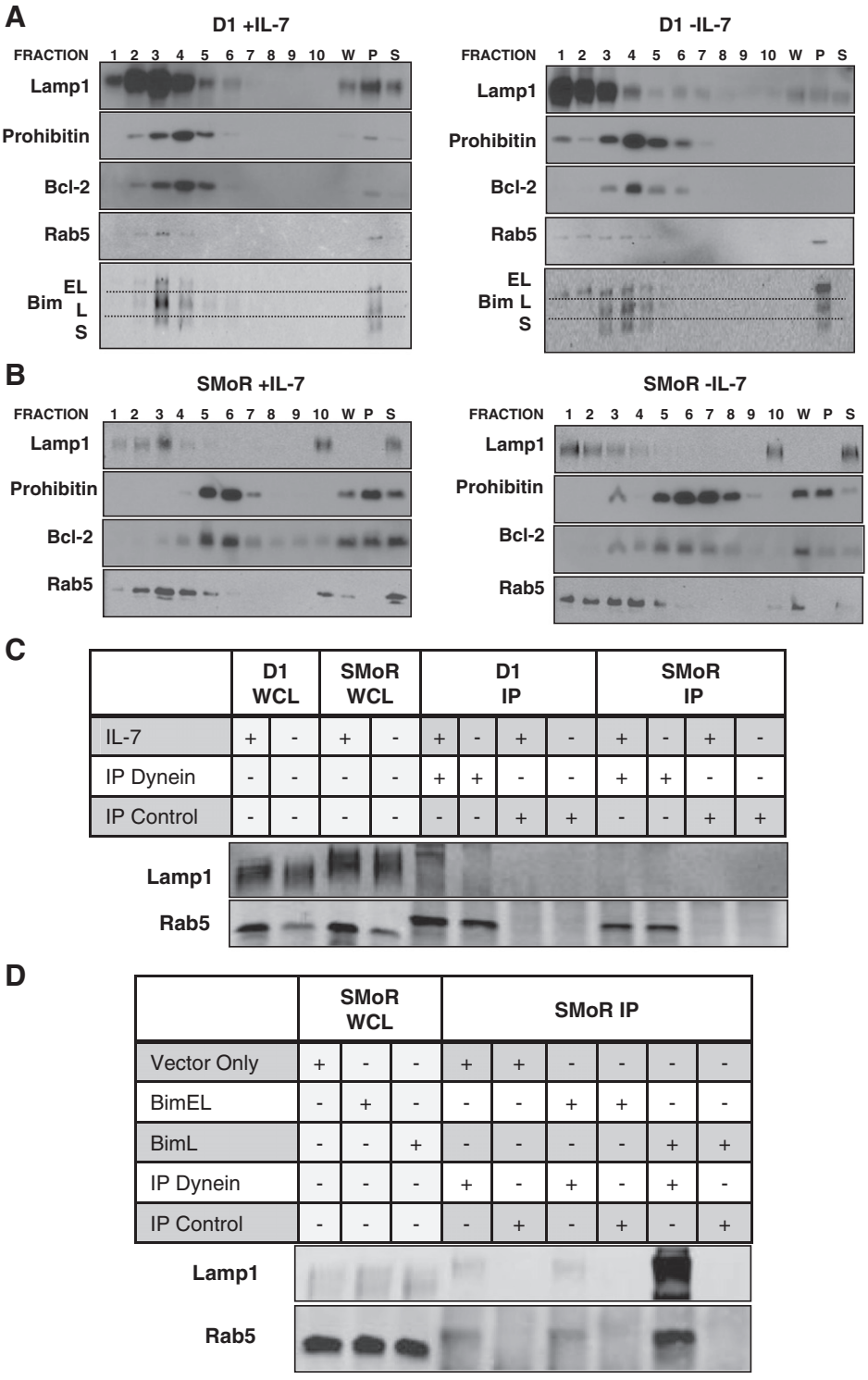

Fig. 7. BimL associates with lysosomes through interactions with dynein. (A) A representative immunoblot is shown of lysates enriched for lysosomal content from D1 cells. D1 cells were cultured in the presence or absence of IL-7 for 20 h and subjected to differential ultracentrifugation. Gradient fractions (17–30% Optiprep fractions, fractions 1–10), whole cell lysate (W), pellets after initial centrifugation step (P), and supernatant after initial centrifugation (S), were immunoblotted for Lamp1 (late endosome and lysosomal membrane), prohibitin (mitochondria), Rab5 (early endosome), Bcl-2, and Bim. (B) Enriched lysosomal protein lysates which were prepared from SMoR cells cultured in the presence or absence of IL-7 for 20 h as described for D1 cells above (A) were analyzed by immunoblot. Blots are representative of nine independent experiments. (C) Immunoblots show co-immunoprecipitation of dynein with Lamp1 upon presence of BimL. As input controls, the whole cell lysates before immunoprecipitation are included. Whole cell lysates of D1 and SMoR cells were cultured with or without IL-7 for 20 h incubated with either dynein or control antibody to co-immunoprecipitate binding proteins, subjected to SDS-PAGE and immunoblotted for lysosomal/late endosomal protein (Lamp1), and early endosomal content (Rab5). (D) Whole cell lysates of SMoR cells transfected with retrovirus to express individual Bim isoforms as described in Materials and methods, co-immunoprecipitated with either dynein or control antibody, were immunoblotted for lysosomal/late endosomal protein (Lamp1), early endosomal protein (Rab5), and Bim. For immunoblots displayed in B-D, a representative experiment of three performed is shown. Images from full-length blots were cropped for concise presentation.

protein in non-apoptotic cells [18,67]. To determine whether Bim facilitated the binding of lysosomes to dynein, we performed a co-immunoprecipitation experiment. Lysates were prepared from D1 cells cultured with IL-7 and immunoprecipitated with an anti-dynein antibody. Blots were probed for Lamp1 as indicator of lysosome cargo. As shown in Fig. 7C, dynein co-immunoprecipitated with Lamp1 in D1 cells grown with IL-7. We could not co-immunoprecipitate dynein with Lamp1 in SMoR cells grown with or without IL-7 or with D1 cells deprived of IL-7 — basically, cells lacking or with reduced content of BimL. As control, we found that Rab5 associated with dynein independently of IL-7 or Bim (Fig. 7C). Additionally, we observed that all the immunoprecipitated versions of Lamp1 and Rab5 ran slightly slower on the gels indicating possible modifications that enable complex formation. Also, the stronger detection of Lamp1 in the input lanes for SMoR cells as compared to other blots was due to significantly increased amount of protein input used to maximize detection of co-immunoprecipitates.

Next, BimEL and BimL were expressed in SMoR cells using a retroviral method. This method necessitated reduced numbers of cells as compared to blots in Fig. 7A–C. Shown in the representative experiment in Fig. 7D, we found that expression of BimL, but not BimEL, was able to restore the interaction of dynein with Lamp1-containing vesicles in SMoR cells, significantly increasing the detection of Lamp1 (and some Rab5) well above endogenous levels. Thus, BimL could function as an adaptor for dynein to facilitate the loading and fusion of lysosomes within cells.

The role of BimL, as mediator of lysosomal positioning through its interaction with dynein, was examined by expressing the three isoforms of Bim in SMoR cells, and observing the effects upon lysosomal distribution and cell viability. To perform these experiments we used the probe, LysoTracker. Because we were imaging GFP positive cells to track those that were expressing the isoforms of Bim, we could not use LysoSensor as in Fig. 3 since the fluorescent signals overlapped. We used the same live cell imaging technique as shown in Fig. 3. In addition, in each image set, a dot plot displays cell death measured by Sytox uptake and membrane asymmetry. Images were collected at the final experimental time point. Results in Fig. 8A demonstrated that SMoR cells expressing the empty vector, pMIG, had dim LysoTracker staining, and viability upon retroviral expression was 62%. When BimEL was expressed, we noticed some lysosomal staining with little or no vesicle aggregation (Fig. 8B), and viability decreased to 45%. In contrast, expression of BimL resulted in notable lysosomal aggregation, likely indicative of fusion (Fig. 8C), with viability stable at about 49–50%. For comparison, we also expressed BimS, which was the most toxic of the isoforms, causing rapid cell death with most of the GFP positive cells in the field acquiring a shrunken and apoptotic morphology (Fig. 8D), and viability dropping to 30%.

4. Discussion

In this study, using Bim-containing and Bim-deficient T-cells, we examined the function of Bim during apoptosis and the degradative phase of autophagy controlled by IL-7 stimulation and determined that the major isoforms of Bim contribute independently to these processes. We found that BimL may facilitate lysosomal positioning in cells responding to IL-7 through interactions with dynein. We also observed that loss of IL-7 up-regulated total Bim transcription, and that Bim deficiency partially protected these cells from death induced by IL-7 withdrawal, suggesting that the other isoforms participated in the intrinsic pathway of apoptosis. In support, we found that T-cells lacking functional Bim had decreased growth rate, increased endosomal and reduced lysosomal content, and were resistant to the effects of cathepsin inhibition or impairment of lysosomal acidification. Over-expression of BimL in Bim deficient cells increased vesicular aggregation, while BimEL, and more so BimS, overexpression increased apoptotic morphology. Taken together, these results demonstrated that the major isoforms of Bim could have distinct activities in T-cells that were indicated by localization to different organelles.

Based on our studies, and others, it can be surmised that T-cells lacking Bim would be deficient in the ability of lysosomes to degrade intracellular contents. Hence, Bim-deficient T-cells would not effectively degrade autophagic vesicles or initiate lysosome-mediated apoptotic events [68]. As a result, Bim deficient T-cells could be delayed from undergoing cell death, but, lacking the lysosomal degradative machinery, they would eventually succumb perhaps to nutrient deprivation or metabolic suicide. It is also possible that a limited form of autophagy could occur in the absence of Bim. Under some conditions, the contents of autophagic vesicles can be degraded by amphisomes, autophagic vacuoles formed through the fusion of endosomes to autophagosomes [69]. In Bim-deficient cells, we detected increased amounts of Rab5, an early endosome marker, suggesting that the fusion of early endosomes was possible and could, during autophagy, perhaps form amphisomes in the absence of forming autolysosomes. There is also the possibility that with reduced lysosomal activities, degradation via the proteosome could be impaired [70]. p62 is primarily degraded by lysosomes and proteasomes [71], hence, this could explain why incomplete degradation and accumulation of p62 occurs, and why CQ and 3-MA treatments have little effect on Bim deficient SMoR cells.

Previous studies demonstrated that Bim is sequestered by dynein in healthy cells, and dissociates upon an apoptotic stimulus; providing a possible regulatory mechanism for the protein's apoptotic activity [18,72]. However, the viability of T cells transfected with a BH3 domain mutant of BimL was increased [32]. This suggested a possibility that beyond sequestering Bim, the interaction of BimL with dynein facilitates the loading and perhaps fusion and positioning of lysosomes. In our study, IL-7 withdrawal induced vesicular aggregation in T-cells containing Bim, while this was not observed in Bim deficient T-cells. This result is supported by studies with dynein-deficient cells in which endosomal and lysosomal content became dispersed and lysosomes ceased to co-localize with microtubules [73,74]. Moreover, knockdown of Huntingtin (Htt), a scaffolding protein that interacts with dynein, resulted in lysosomal accumulation and aggregation, indicating that Htt was involved in the movement of cargo. In contrast, we found that Bim deficiency resulted in dispersed vesicles and reduced aggregation, suggesting that Bim's role may not be in cargo movement but rather in facilitating the fusion of late endosomes/lysosomes. An example similar to Bim deficiency was seen in a study using mice deficient in Snapin, a SNARE-binding protein. Deletion of Snapin caused accumulation of endocytic organelles and impaired lysosomal function and maturity [75]. These results support the possibility that the dynein-binding motif on Bim, KXTQT [19], renders the protein accessible as an adaptor for dynein during normal T-cell function to facilitate the positioning and fusion of lysosomal cargo.

The regulation of Bim transcription is mediated by the forkhead transcription factor, FKHR-L1, in growth factor-deprived hematopoietic cells [23,76]. This transcription factor, also known as Foxo3a, translocates to the nucleus when the PI3-kinase/Akt pathway is down-regulated in the absence of survival signals [77]. In neurons, under growth factor deprivation, Bim was up-regulated but required Jun N-terminal protein kinases (JNK) activation [67,78]. We show that IL-7 induced basal levels of *bim* gene transcription, even in non-apoptotic cells, and that the withdrawal of IL-7 further amplified Bim synthesis. It may be that the JNK pathway and the PI3K pathway, both shown to be active in response to IL-7 signaling [38,79,80], may contribute to Bim expression in T-cells. Interestingly, engagement of IL-7 induces the internalization and further recycling of the IL-7R by proteasomes and lysosomes [81–83]. It is possible that Bim, by enabling lysosomal degradative activities, could play a role in regulating the amount of IL-7R available for membrane expression. In support,

we found that in SMoR cells IL-7R levels were slightly higher. Further evidence comes from a study in which cells were cultured with IL-7 and treated with a clathrin formation inhibitor [81]. As a result, pAKT was reduced, which in turn, stimulated FKHR-1 translocation and increased Bim synthesis, perhaps to participate in the maintenance of IL-7R recycling [81].

Another way of controlling Bim levels includes regulation of alternative mRNA splicing. For example, in B cells, engagement of the B

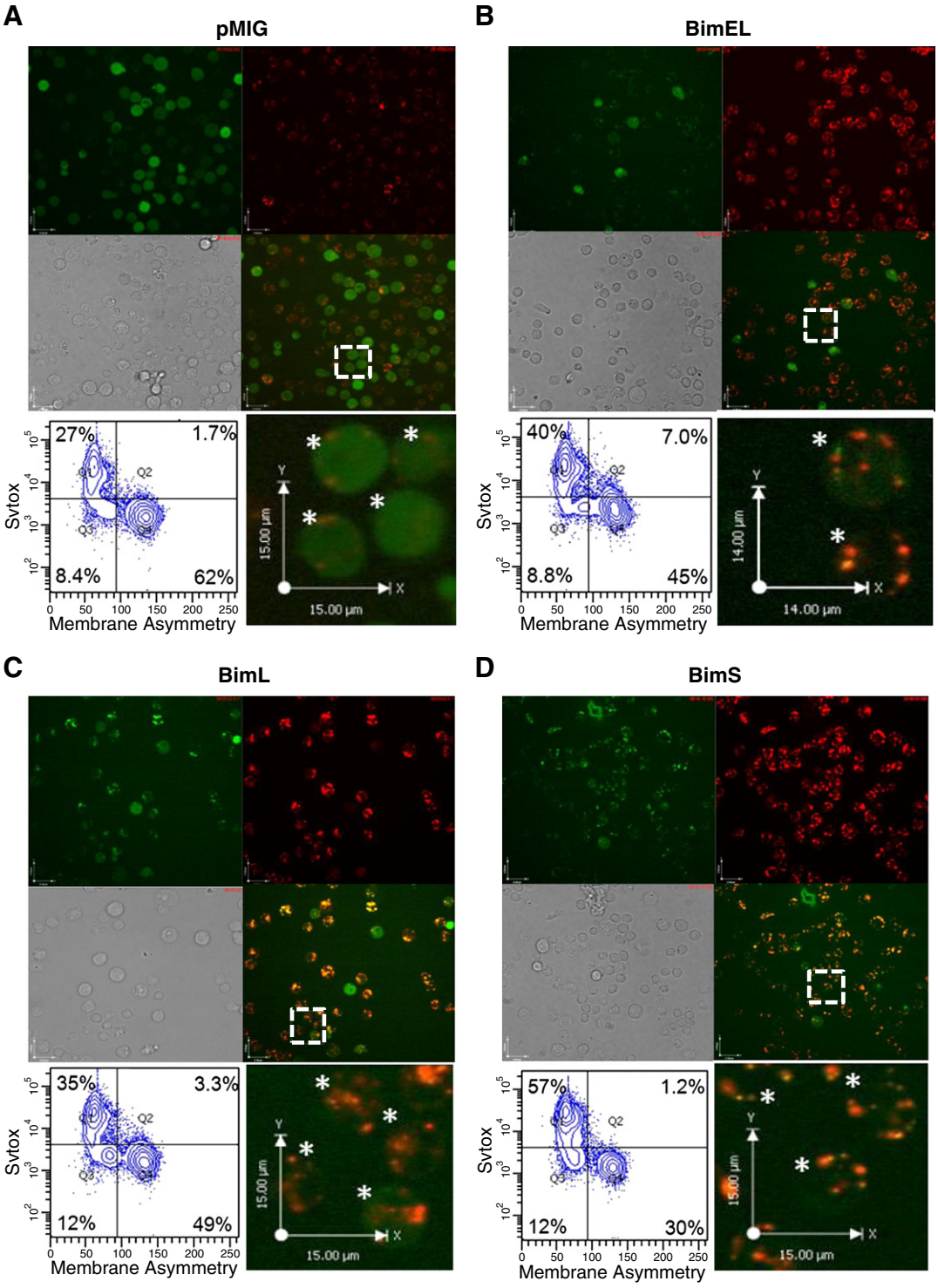

Fig. 8. Expression of BimL restores lysosomal distribution in SMoR cells. Live cell confocal microscopy images of SMoR cells are shown. Images are representative "snapshots" taken at the end of a 24 h live-imaging experiment. SMoR cells were retrovirally transfected to express the control plasmid, pMIG (A), or the individual Bim isoforms, BimEL (B), BimL (C) and BimS (D), in the presence of IL-7, and loaded with 1 μM LysoTracker. Images were acquired using the UltraView spinning disk confocal system (PerkinElmer) with AxioObserver.Z1 (Carl Zeiss) stand, and a Plan-Apochromat 40×/1.4 Oil DIC objective. Each field contains the same cells but with different fluorescent channels: GFP fluorescence (upper left), RFP (LysoTracker) fluorescence (upper right), DIC (lower left), and overlay of GFP and RFP (LysoTracker) fluorescence (lower right). Each panel also contains a larger, digitally magnified inset of the overlay, as indicated by a white cutout within the overlay panel. The magnification inset contains transfected cells indicated by (*). The bottom left panel of each figure section is a density plot displaying the viability of SMoR cells expressing control or Bim isoforms. Cell death was assessed by Sytox uptake (membrane permeability) and membrane asymmetry. Dot plots show percentages representing the population of cells that are non-apoptotic (lower right quadrant), early apoptotic (lower left quadrant) or late apoptotic/necrotic (upper left quadrant). Quadrants were established using controls. Results shown are representative of three experiments.

cell receptor (BCR) led to BimL expression not through increased generation of BimL mRNA but rather through splicing of the BimEL mRNA. Hence BimEL was a pre-mRNA form of BimL [84]. Additionally, deletion of exons containing phosphorylation sites, which are involved in alternative splicing, can contribute to BimL expression. As an example, in BimEL mutant mice lacking exon 3 which encodes sites of MAPK phosphorylation, an increase in BimL protein expression occurred [29]. In our study, we observed more BimL protein compared to BimEL in the presence of IL-7, suggesting that BimL was being produced in preference to BimEL, perhaps through the splicing mechanism described above. In the absence of IL-7, we noted increased total Bim mRNA and more BimEL protein, indicating that the possible splicing of BimEL to make BimL may only be occurring upon an IL-7 stimulus.

Our results indicated that the BimL isoform has a non-apoptotic activity that supports lysosome maintenance. Bim and IL-7R double-deficient mice showed partial restoration of thymocyte development [17], while, in a bone marrow chimera, Bim deficiency failed to fully reconstitute thymocyte development [31]. Bim deficiency, in our studies, failed to rescue adoptively transferred T-cells in IL-7$^{-/-}$ hosts. The inability of Bim deficiency to completely restore an immunodeficient phenotype could in part be explained by the redundancy of other pro-apoptotic proteins like Bad or Bid. However, another perspective could be that Bim isoforms have both apoptosis (BimEL, and BimS) and cell maintenance or autophagic (BimL) activities. Other apoptosis-regulating proteins have been shown to contribute to autophagy. For example, anti-apoptotic Bcl-2 bound Beclin-1 and inhibited autophagic induction, but overexpression of pro-apoptotic protein, Bad, induced autophagy in human cells [85]. Additionally, the lone *Caenorhabditis elegans* BH3-only protein, EGL-1, can trigger autophagy [86]. In studies examining the individual isoforms of Bim, in which both BimL and Bcl-2 were expressed, BimL could not overcome the anti-apoptotic effects of Bcl-2 [87], perhaps because BimL could not perform its non-apoptotic function as we have described. Moreover, over-expression of BimL did not cause release of cytochrome c [87].

The implications of Bim isoforms having different cellular activities for disease treatments are significant. In cancers with specific genetic mutations, Bim levels were found to be predictive of the effect of inhibitors targeting PI3K, HER2 or EGFR, but did not correlate with effectiveness to standard chemotherapeutics [88]. Efforts at developing inhibitory Bim BH3-like mimetics for therapy only consider the pro-apoptotic action of Bim mediated, for example, through the BH3 domain [89]. Our work suggests that Bim may be more complex, having multiple isoforms and functions. An alternative approach could be the design of compounds that target the Bim isoform-splicing mechanisms. As a result, one could potentially control the generation of a specific isoform to elicit the desired apoptotic (BimEL/S > BimL) or autophagic (BimL > BimEL/S) outcome in a manner that is more effective than the targeting of total Bim.

5. Conclusions

In summary, our results revealed that the major isoforms of Bim has defined functions in the cell maintenance and the apoptotic process occurring in T-cells responsive to IL-7. In T-cells receiving an IL-7 signal, BimL plays an essential role in lysosomal positioning through interactions with dynein that enable the formation of autolysosomes during the degradative phase of autophagy. BimEL associates with mitochondria in a pro-apoptotic manner, and expression of BimS further promotes the cell death process. BimL, therefore, functions in the presence of IL-7 to support lysosomal acidification, while BimEL and BimS are active during IL-7 deprivation to promote T-cell apoptosis.

Acknowledgements

This study was supported by an NIH/NCI grant CA109524RO1 (Khaled) from the National Institutes of Health (NIH).

Appendix A. Supplementary data

Supplementary data to this article can be found online at http://dx.doi.org/10.1016/j.bbamcr.2012.06.017.

References

[1] A. Gross, J.M. Mcdonnell, S.J. Korsmeyer, Bcl-2 family members and the mitochondria in apoptosis, Genes Dev. 13 (1999) 1899–1911.
[2] D.A. Hildeman, Y. Zhu, T.C. Mitchell, P. Bouillet, A. Strasser, J. Kappler, P. Marrack, Activated T cell death in vivo mediated by proapoptotic Bcl-2 family member Bim, Immunity 16 (2002) 759–767.
[3] A.L. Snow, J.B. Oliveira, L. Zheng, J.K. Dale, T.A. Fleisher, M.J. Lenardo, Critical role for Bim in T cell receptor restimulation-induced death, Biol. Direct 3 (2008) 34.
[4] J.C. Rathmell, M.G. Vander Heiden, M.H. Harris, K.A. Frauwirth, C.B. Thompson, In the absence of extrinsic signals, nutrient utilization by lymphocytes is insufficient to maintain either cell size or viability, Mol. Cell 6 (2000) 683–692.
[5] Y. Sawa, Y. Arima, H. Ogura, C. Kitabayashi, J.J. Jiang, T. Fukushima, D. Kamimura, T. Hirano, M. Murakami, Hepatic interleukin-7 expression regulates T cell responses, Immunity 30 (2009) 447–457.
[6] R.I. Mazzucchelli, S. Warming, S.M. Lawrence, M. Ishii, M. Abshari, A.V. Washington, L. Feigenbaum, A.C. Warner, D.J. Sims, W.Q. Li, J.A. Hixon, D.H. Gray, B.E. Rich, M. Morrow, M.R. Anver, J. Cherry, D. Naf, L.R. Sternberg, D.W. Mcvicar, A.G. Farr, R.N. Germain, K. Rogers, N.A. Jenkins, N.G. Copeland, S.K. Durum, Visualization and identification of IL-7 producing cells in reporter mice, PLoS One 4 (2009) E7637.
[7] G.Y. Kim, C. Hong, J.H. Park, Seeing is believing: illuminating the source of in vivo interleukin-7, Immune Netw. 11 (2011) 1–10.
[8] Q. Jiang, W.Q. Li, F.B. Aiello, R. Mazzucchelli, B. Asefa, A.R. Khaled, S.K. Durum, Cell biology of IL-7, A key lymphotrophin, Cytokine Growth Factor Rev. 16 (2005) 513–533.
[9] U. Von-Freeden-Jeffry, P. Vieira, L.A. Lucian, T. Mcneil, S.E. Burdach, R. Murray, Lymphopenia in interleukin (IL)-7 gene-deleted mice identifies IL-7 as a nonredundant cytokine, J. Exp. Med. 181 (1995) 1519–1526.
[10] E. Maraskovsky, M. Teepe, P.J. Morrissey, S. Braddy, R.E. Miller, D.H. Lynch, J.J. Peschon, Impaired survival and proliferation in IL-7 receptor-deficient peripheral T cells, J. Immunol. 157 (1996) 5315–5323.
[11] S.Y. Lai, J. Molden, M.A. Goldsmith, Shared gamma(C) subunit within the human interleukin-7 receptor complex. a molecular basis for the pathogenesis of X-linked severe combined immunodeficiency, J. Clin. Invest. 99 (1997) 169–177.
[12] B.E. Rich, J. Campos-Torres, R.I. Tepper, R.W. Moreadith, P. Leder, Cutaneous lymphoproliferation and lymphomas in interleukin 7 transgenic mice, J. Exp. Med. 177 (1993) 305–316.
[13] K. Yamanaka, R. Clark, B. Rich, R. Dowgiert, K. Hirahara, D. Hurwitz, M. Shibata, N. Mirchandani, D.A. Jones, D.S. Goddard, S. Eapen, H. Mizutani, T.S. Kupper, Skin-derived interleukin-7 contributes to the proliferation of lymphocytes in cutaneous T-cell lymphoma, Blood 107 (2006) 2440–2445.
[14] J.T. Tan, E. Dudl, E. Leroy, R. Murray, J. Sprent, K.I. Weinberg, C.D. Surh, IL-7 is critical for homeostatic proliferation and survival of naive T cells, Proc. Natl. Acad. Sci. U. S. A. 98 (2001) 8732–8737.
[15] E. Maraskovsky, J.J. Peschon, H. Mckenna, M. Teepe, A. Strasser, Overexpression of Bcl-2 does not rescue impaired B lymphopoiesis in IL-7 receptor-deficient mice but can enhance survival of mature B cells, Int. Immunol. 10 (1998) 1367–1375.
[16] A.R. Khaled, K. Kim, R. Hofmeister, K. Muegge, S.K. Durum, Withdrawal of IL-7 induces Bax translocation from cytosol to mitochondria through a rise in intracellular pH, Proc. Natl. Acad. Sci. U. S. A. 96 (1999) 14476–14481.
[17] M. Pellegrini, P. Bouillet, M. Robati, G.T. Belz, G.M. Davey, A. Strasser, Loss of Bim increases T cell production and function in interleukin 7 receptor-deficient mice, J. Exp. Med. 200 (2004) 1189–1195.
[18] H. Puthalakath, D.C. Huang, L.A. O'reilly, S.M. King, A. Strasser, The proapoptotic activity of the Bcl-2 family member Bim is regulated by interaction with the dynein motor complex, Mol. Cell 3 (1999) 287–296.
[19] G. Benison, P.A. Karplus, E. Barbar, Structure and dynamics of LC8 complexes with KXTQT-motif peptides: swallow and dynein intermediate chain compete for a common site, J. Mol. Biol. 371 (2007) 457–468.
[20] Y. Zhu, B.J. Swanson, M. Wang, D.A. Hildeman, B.C. Schaefer, X. Liu, H. Suzuki, K. Mihara, J. Kappler, P. Marrack, Constitutive association of the proapoptotic protein Bim with Bcl-2-related proteins on mitochondria in T cells, Proc. Natl. Acad. Sci. U. S. A. 101 (2004) 7681–7686.
[21] P.F. Dijkers, K.U. Birkenkamp, E.W. Lam, N.S. Thomas, J.W. Lammers, L. Koenderman, P.J. Coffer, Fkhr-L1 can act as a critical effector of cell death induced by cytokine withdrawal: protein kinase B-enhanced cell survival through maintenance of mitochondrial integrity, J. Cell Biol. 156 (2002) 531–542.
[22] M. Stahl, P.F. Dijkers, G.J. Kops, S.M. Lens, P.J. Coffer, B.M. Burgering, R.H. Medema, The forkhead transcription factor Foxo regulates transcription of P27kip1 and Bim in response to IL-2, J. Immunol. 168 (2002) 5024–5031.
[23] T. Yano, K. Ito, H. Fukamachi, X.Z. Chi, H.J. Wee, K. Inoue, H. Ida, P. Bouillet, A. Strasser, S.C. Bae, Y. Ito, The Runx3 tumor suppressor upregulates Bim in gastric epithelial cells undergoing transforming growth factor beta-induced apoptosis, Mol. Cell. Biol. 26 (2006) 4474–4488.
[24] K. Lei, R.J. Davis, JNK phosphorylation of Bim-related members of the Bcl2 family induces Bax-dependent apoptosis, Proc. Natl. Acad. Sci. U. S. A. 100 (2003) 2432–2437.
[25] R. Ley, K.E. Ewings, K. Hadfield, E. Howes, K. Balmanno, S.J. Cook, Extracellular signal-regulated kinases 1/2 are serum-stimulated "Bim(EL) kinases" that bind

to the Bh3-only protein Bim(EL) causing its phosphorylation and turnover, J. Biol. Chem. 279 (2004) 8837–8847.
[26] R.J. Seward, P.D. Von Haller, R. Aebersold, B.T. Huber, Phosphorylation of the pro-apoptotic protein Bim in lymphocytes is associated with protection from apoptosis, Mol. Immunol. 39 (2003) 983–993.
[27] F. Luciano, A. Jacquel, P. Colosetti, M. Herrant, S. Cagnol, G. Pages, P. Auberger, Phosphorylation of Bim-EL by Erk1/2 on serine 69 promotes its degradation via the proteasome pathway and regulates its proapoptotic function, Oncogene 22 (2003) 6785–6793.
[28] C.R. Weston, K. Balmanno, C. Chalmers, K. Hadfield, S.A. Molton, R. Ley, E.F. Wagner, S.J. Cook, Activation of Erk1/2 by deltaraf-1:Er* represses Bim expression independently of the JNK or Pi3k pathways, Oncogene 22 (2003) 1281–1293.
[29] A. Hubner, T. Barrett, R.A. Flavell, R.J. Davis, Multisite phosphorylation regulates Bim stability and apoptotic activity, Mol. Cell 30 (2008) 415–425.
[30] K.T. Leung, K.K. Li, S.S. Sun, P.K. Chan, V.E. Ooi, L.C. Chiu, Activation of the JNK pathway promotes phosphorylation and degradation of BimEL—a novel mechanism of chemoresistance in T-cell acute lymphoblastic leukemia, Carcinogenesis 29 (2008) 544–551.
[31] W.Q. Li, T. Guszczynski, J.A. Hixon, S.K. Durum, Interleukin-7 regulates Bim proapoptotic activity in peripheral T-cell survival, Mol. Cell. Biol. 30 (2010) 590–600.
[32] L. O'Connor, A. Strasser, L.A. O'Reilly, G. Hausmann, J.M. Adams, S. Cory, D.C. Huang, Bim: a novel member of the Bcl-2 family that promotes apoptosis, EMBO J. 17 (1998) 384–395.
[33] U.M.T. Miyashita, Y. Shikama, K. Tadokoro, M. Yamada, Molecular cloning and characterization of six novel isoforms of human Bim, a member of the proapoptotic Bcl-2 family, FEBS Lett. 509 (2001) 135–141.
[34] M. Adachi, X. Zhao, K. Imai, Nomenclature of dynein light chain-linked Bh3-only protein Bim isoforms, Cell Death Differ. 12 (2005) 192–193.
[35] V.M. Hubbard, R. Valdor, B. Patel, R. Singh, A.M. Cuervo, F. Macian, Macroautophagy regulates energy metabolism during effector T cell activation, J. Immunol. 185 (2010) 7349–7357.
[36] C. Li, E. Capan, Y. Zhao, J. Zhao, D. Stolz, S.C. Watkins, S. Jin, F. Macian, Autophagy is induced in Cd4+ T cells and important for the growth factor-withdrawal cell death, J. Immunol. 177 (2006) 5163–5168.
[37] K. Kim, A.R. Khaled, D. Reynolds, H.A. Young, C.K. Lee, S.K. Durum, Characterization of an interleukin-7-dependent thymic cell line derived from a P53(−/−) mouse, J. Immunol. Methods 274 (2003) 177–184.
[38] W.Q. Li, Q. Jiang, A.R. Khaled, J.R. Keller, S.K. Durum, Interleukin-7 inactivates the pro-apoptotic protein Bad promoting T cell survival, J. Biol. Chem. 279 (2004) 29160–29166.
[39] Q. Jiang, W.Q. Li, R.R. Hofmeister, H.A. Young, D.R. Hodge, J.R. Keller, A.R. Khaled, S.K. Durum, Distinct regions of the interleukin-7 receptor regulate different Bcl2 family members, Mol. Cell. Biol. 24 (2004) 6501–6513.
[40] A.R. Khaled, D.V. Bulavin, C. Kittipatarin, W.Q. Li, M. Alvarez, K. Kim, H.A. Young, A.J. Fornace, S.K. Durum, Cytokine-driven cell cycling is mediated through Cdc25a, J. Cell Biol. 169 (2005) 755–763.
[41] M. Chehtane, A.R. Khaled, Interleukin-7 mediates glucose utilization in lymphocytes through transcriptional regulation of the Hexokinase II gene, Am. J. Physiol. Cell Physiol. 298 (2010) C1560–C1571.
[42] C. Kittipatarin, A.R. Khaled, Ex vivo expansion of memory CD8 T cells from lymph nodes or spleen through in vitro culture with interleukin-7, J. Immunol. Methods 344 (2009) 45–57.
[43] C. Kittipatarin, N. Tschammer, A.R. Khaled, The interaction of LCK and the CD4 co-receptor alters the dose response of T-cells to interleukin-7, Immunol. Lett. 131 (2010) 170–181.
[44] C. Kittipatarin, W. Li, S.K. Durum, A.R. Khaled, Cdc25a-driven proliferation regulates Cd62l levels and lymphocyte movement in response to interleukin-7, Exp. Hematol. 38 (2010) 1143–1156.
[45] A.L. Grenier, K. Bu-Ihweij, G. Zhang, S. Moore, R. Boohaker, E. Slepkov, K. Pridemore, J.J. Ren, L. Fliegel, A.R. Khaled, Apoptosis-induced alkalinization by the Na+/H+ exchanger isoform 1 is mediated through phosphorylation of amino acids Ser726 and Ser729, Am. J. Physiol. Cell Physiol. 295 (2008) C883–C896.
[46] P. Franck, N. Petitipain, M. Cherlet, M. Dardennes, F. Maachi, B. Schutz, L. Poisson, P. Nabet, Measurement of intracellular pH in cultured cells by flow cytometry with BCECF, Am. J Biotechnol. 46 (1996) 187–195.
[47] S.N. Willis, J.M. Adams, Life in the balance: how Bh3-only proteins induce apoptosis, Curr. Opin. Cell Biol. 17 (2005) 617–625.
[48] B. Seddon, R. Zamoyska, TCR and IL-7 receptor signals can operate independently or synergize to promote lymphopenia-induced expansion of naive T cells, J. Immunol. 169 (2002) 3752–3759.
[49] W.Q. Li, Q. Jiang, E. Aleem, P. Kaldis, A.R. Khaled, S.K. Durum, IL-7 promotes T cell proliferation through destabilization of P27kip1, J. Exp. Med. 203 (2006) 573–582.
[50] A.R. Khaled, S.K. Durum, Death and baxes: mechanisms of lymphotrophic cytokines, Immunol. Rev. 193 (2003) 48–57.
[51] H.C. Reinhardt, B. Schumacher, The P53 network: cellular and systemic DNA damage responses in aging and cancer, Trends Genet. 28 (2012) 128–136.
[52] P.G. Komarov, E.A. Komarova, R.V. Kondratov, K. Christov-Tselkov, J.S. Coon, M.V. Chernov, A.V. Gudkov, A chemical inhibitor of P53 that protects mice from the side effects of cancer therapy, Science 285 (1999) 1733–1737.
[53] D. Sohn, V. Graupner, D. Neise, F. Essmann, K. Schulze-Osthoff, R.U. Janicke, Pifithrin-alpha protects against DNA damage-induced apoptosis downstream of mitochondria independent of P53, Cell Death Differ. 16 (2009) 869–878.
[54] R. Mazzucchelli, S.K. Durum, Interleukin-7 receptor expression: intelligent design, Nat. Rev. Immunol. 7 (2007) 144–154.
[55] B. Turk, V. Turk, Lysosomes as "suicide bags" in cell death: myth or reality? J. Biol. Chem. 284 (2009) 21783–21787.
[56] C. Nilsson, U. Johansson, A.C. Johansson, K. Kagedal, K. Ollinger, Cytosolic acidification and lysosomal alkalinization during TNF-alpha induced apoptosis in U937 cells, Apoptosis 11 (2006) 1149–1159.
[57] S.F. Pedersen, The Na (+)/H (+) exchanger Nhe1 in stress-induced signal transduction: implications for cell proliferation and cell death, Pflugers Arch. 452 (2006) 249–259.
[58] R.A. Gonzalez-Polo, M. Niso-Santano, M.A. Ortiz-Ortiz, A. Gomez-Martin, J.M. Moran, L. Garcia-Rubio, J. Francisco-Morcillo, C. Zaragoza, G. Soler, J.M. Fuentes, Inhibition of paraquat-induced autophagy accelerates the apoptotic cell death in neuroblastoma Sh-Sy5y cells, Toxicol. Sci. 97 (2007) 448–458.
[59] H.M. Shen, P. Codogno, Autophagic cell death: Loch Ness monster or endangered species? Autophagy 7 (2011).
[60] Y.T. Wu, H.L. Tan, G. Shui, C. Bauvy, Q. Huang, M.R. Wenk, C.N. Ong, P. Codogno, H.M. Shen, Dual role of 3-methyladenine in modulation of autophagy via different temporal patterns of inhibition on class I and III phosphoinositide 3-kinase, J. Biol. Chem. 285 (2010) 10850–10861.
[61] Y. Kabeya, N. Mizushima, T. Ueno, A. Yamamoto, T. Kirisako, T. Noda, E. Kominami, Y. Ohsumi, T. Yoshimori, LC3, a mammalian homologue of yeast Apg8p, is localized in autophagosome membranes after processing, EMBO J. 19 (2000) 5720–5728.
[62] Y. Kabeya, N. Mizushima, A. Yamamoto, S. Oshitani-Okamoto, Y. Ohsumi, T. Yoshimori, LC3, Gabarap and Gate16 localize to autophagosomal membrane depending on form-II formation, J. Cell Sci. 117 (2004) 2805–2812.
[63] E. Itakura, N. Mizushima, P62 targeting to the autophagosome formation site requires self-oligomerization but not LC3 binding, J. Cell Biol. 192 (2011) 17–27.
[64] A. Gonzalez-Noriega, J.H. Grubb, V. Talkad, W.S. Sly, Chloroquine inhibits lysosomal enzyme pinocytosis and enhances lysosomal enzyme secretion by impairing receptor recycling, J. Cell Biol. 85 (1980) 839–852.
[65] Y. He, Y. Xu, C. Zhang, X. Gao, K.J. Dykema, K.R. Martin, J. Ke, E.A. Hudson, S.K. Khoo, J.H. Resau, A.S. Alberts, J.P. Mackeigan, K.A. Furge, H.E. Xu, Identification of a lysosomal pathway that modulates glucocorticoid signaling and the inflammatory response, Sci. Signal. 4 (2011) Ra44.
[66] P.J. Meikle, D.A. Brooks, E.M. Ravenscroft, M. Yan, R.E. Williams, A.E. Jaunzems, T.K. Chataway, L.E. Karageorgos, R.C. Davey, C.D. Boulter, S.R. Carlsson, J.J. Hopwood, Diagnosis of lysosomal storage disorders: evaluation of lysosome-associated membrane protein LAMP-1 as a diagnostic marker, Clin. Chem. 43 (1997) 1325–1335.
[67] G.V. Putcha, S. Le, S. Frank, C.G. Besirli, K. Clark, B. Chu, S. Alix, R.J. Youle, A. Lamarche, A.C. Maroney, E.M. Johnson Jr., JNK-mediated Bim phosphorylation potentiates Bax-dependent apoptosis, Neuron 38 (2003) 899–914.
[68] G. Droga-Mazovec, L. Bojic, A. Petelin, S. Ivanova, R. Romih, U. Repnik, G.S. Salvesen, V. Stoka, V. Turk, B. Turk, Cysteine cathepsins trigger caspase-dependent cell death through cleavage of Bid and antiapoptotic Bcl-2 homologues, J. Biol. Chem. 283 (2008) 19140–19150.
[69] T.O. Berg, M. Fengsrud, P.E. Stromhaug, T. Berg, P.O. Seglen, Isolation and characterization of rat liver amphisomes. Evidence for fusion of autophagosomes with both early and late endosomes, J. Biol. Chem. 273 (1998) 21883–21892.
[70] L. Qiao, J. Zhang, Inhibition of lysosomal functions reduces proteasomal activity, Neurosci. Lett. 456 (2009) 15–19.
[71] S. Isogai, D. Morimoto, K. Arita, S. Unzai, T. Tenno, J. Hasegawa, Y.S. Sou, M. Komatsu, K. Tanaka, M. Shirakawa, H. Tochio, Crystal structure of the ubiquitin-associated (UBA) domain of P62 and its interaction with ubiquitin, J. Biol. Chem. 286 (2011) 31864–31874.
[72] C.L. Day, H. Puthalakath, G. Skea, A. Strasser, I. Barsukov, L.Y. Lian, D.C. Huang, M.G. Hinds, Localization of dynein light chains 1 and 2 and their pro-apoptotic ligands, Biochem. J. 377 (2004) 597–605.
[73] A. Harada, Y. Takei, Y. Kanai, Y. Tanaka, S. Nonaka, N. Hirokawa, Golgi vesiculation and lysosome dispersion in cells lacking cytoplasmic dynein, J. Cell Biol. 141 (1998) 51–59.
[74] J.P. Caviston, A.L. Zajac, M. Tokito, E.L. Holzbaur, Huntingtin coordinates the dynein-mediated dynamic positioning of endosomes and lysosomes, Mol. Biol. Cell 22 (2011) 478–492.
[75] Q. Cai, L. Lu, J.H. Tian, Y.B. Zhu, H. Qiao, Z.H. Sheng, Snapin-regulated late endosomal transport is critical for efficient autophagy-lysosomal function in neurons, Neuron 68 (2010) 73–86.
[76] P.F. Dijkers, R.H. Medema, J.W. Lammers, L. Koenderman, P.J. Coffer, Expression of the pro-apoptotic Bcl-2 family member Bim is regulated by the forkhead transcription factor FKHR-L1, Curr. Biol. 10 (2000) 1201–1204.
[77] S.R. Datta, A. Brunet, M.E. Greenberg, Cellular survival: a play in three Akts, Genes Dev. 13 (1999) 2905–2927.
[78] J. Whitfield, S.J. Neame, L. Paquet, O. Bernard, J. Ham, Dominant-negative C-Jun promotes neuronal survival by reducing Bim expression and inhibiting mitochondrial cytochrome C release, Neuron 29 (2001) 629–643.
[79] E. Rajnavolgyi, N. Benbernou, K. Muegge, S.K. Durum, IL-7 withdrawal induces a stress pathway activating P38 map kinase and JNK. 2000. Ref Type: Unpublished Work.
[80] A.R. Khaled, W.Q. Li, J. Huang, T.J. Fry, A.S. Khaled, C.L. Mackall, K. Muegge, H.A. Young, S.K. Durum, Bax deficiency partially corrects IL-7 receptor alpha deficiency, Immunity 17 (2002) 561–573.
[81] C.M. Henriques, J. Rino, R.J. Nibbs, G.J. Graham, J.T. Barata, IL-7 induces rapid clathrin-mediated internalization and JAK3-dependent degradation of IL-7ralpha in T cells, Blood 115 (2010) 3269–3277.
[82] L. Swainson, S. Kinet, C. Mongellaz, M. Sourisseau, T. Henriques, N. Taylor, IL-7-induced proliferation of recent thymic emigrants requires activation of the PI3K pathway, Blood 109 (2007) 1034–1042.
[83] I.X. Mcleod, X. Zhou, Q.J. Li, F. Wang, Y.W. He, The class III kinase Vps34 promotes T lymphocyte survival through regulating IL-7ralpha surface expression, J. Immunol. 187 (2011) 5051–5061.

[84] C. Clybouw, A. Hadji, B. Elmchichi, M.T. Auffredou, G. Leca, A. Vazquez, BimL upregulation induced by BCR cross-linking in BL41 Burkitt's lymphoma results from a splicing mechanism of the BimEL mRNA, Biochem. Biophys. Res. Commun. 383 (2009) 32–36.
[85] M.C. Maiuri, T.G. Le, A. Criollo, J.C. Rain, F. Gautier, P. Juin, E. Tasdemir, G. Pierron, K. Troulinaki, N. Tavernarakis, J.A. Hickman, O. Geneste, G. Kroemer, Functional and physical interaction between Bcl-X(L) and a Bh3-like domain in beclin-1, EMBO J. 26 (2007) 2527–2539.
[86] M.C. Maiuri, A. Criollo, E. Tasdemir, J.M. Vicencio, N. Tajeddine, J.A. Hickman, O. Geneste, G. Kroemer, Bh3-only proteins and Bh3 mimetics induce autophagy by competitively disrupting the interaction between beclin 1 and Bcl-2/Bcl-X(L), Autophagy 3 (2007) 374–376.
[87] O. Terradillos, S. Montessuit, D.C. Huang, J.C. Martinou, Direct addition of BimL to mitochondria does not lead to cytochrome C release, FEBS Lett. 522 (2002) 29–34.
[88] A.C. Faber, R.B. Corcoran, H. Ebi, L.V. Sequist, B.A. Waltman, E. Chung, J. Incio, S.R. Digumarthy, S.F. Pollack, Y. Song, A. Muzikansky, E. Lifshits, S. Roberge, E.J. Coffman, C.H. Benes, H.L. Gomez, J. Baselga, C.L. Arteaga, M.N. Rivera, D. As-Santagata, R.K. Jain, J.A. Engelman, Bim expression in treatment-naive cancers predicts responsiveness to kinase inhibitors, Cancer Discov. 1 (2011) 352–365.
[89] J.L. Labelle, S.G. Katz, G.H. Bird, E. Gavathiotis, M.L. Stewart, C. Lawrence, J.K. Fisher, M. Godes, K. Pitter, A.L. Kung, L.D. Walensky, A stapled Bim peptide overcomes apoptotic resistance in hematologic cancers, J. Clin. Invest. 122 (2012) 2018–2031.